HHS Public Access

Author manuscript

ALTEX. Author manuscript; available in PMC 2024 August 07.

Published in final edited form as:

ALTEX. 2024 ; 41(3): 363–381. doi:10.14573/altex.2311031.

A RISK-BASED PRIORITIZATION OF PFAS USING PHENOTYPIC AND TRANSCRIPTOMIC DATA FROM HUMAN INDUCED PLURIPOTENT STEM CELL-DERIVED HEPATOCYTES AND CARDIOMYOCYTES

Han-Hsuan Doris Tsai[1,2], **Lucie C. Ford**[1,2], **Zunwei Chen**[1,2,$], **Allison N. Dickey**[3], **Fred A. Wright**[1,3,4], **Ivan Rusyn**[1,2]

[1]Interdisciplinary Faculty of Toxicology, College Station, Texas 77843, USA

[2]Department of Veterinary Physiology and Pharmacology, Texas A&M University, College Station, Texas 77843, USA

[3]Bioinformatics Research Center, North Carolina State University, Raleigh, NC, USA

[4]Department of Statistics and Bioinformatics Research Center, North Carolina State University, Raleigh, North Carolina 27603, USA

Abstract

Per- and polyfluoroalkyl substances (PFAS) are chemicals with important applications; they are persistent in the environment and may pose human health hazards. Regulatory agencies are considering restrictions and bans of PFAS; however, little data exists for informed decisions. Several prioritization strategies were proposed for evaluation of potential hazards of PFAS. Structure-based grouping could expedite the selection of PFAS for testing; still, the hypothesis that structure-effect relationships exist for PFAS requires confirmation. We tested 26 structurally diverse PFAS from 8 groups using human-induced pluripotent stem cell-derived hepatocytes and cardiomyocytes, and tested concentration-response effects on cell function and gene expression. Few phenotypic effects were observed in hepatocytes, but negative chronotropy was observed for 8 of the 26 PFAS. Substance- and cell type-dependent transcriptomic changes were more prominent but lacked substantial group-specific effects. In hepatocytes, we found up-regulation of stress-related and extracellular matrix organization pathways, and down-regulation of fat metabolism. In cardiomyocytes, contractility-related pathways were most affected. We derived phenotypic and transcriptomic points of departure and compared them to predicted PFAS exposures. The conservative estimates for bioactivity and exposure were used to derive bioactivity-to-exposure ratio (BER) for each PFAS, most (23 of 26) PFAS had BER>1. Overall, these data suggests that structure-based grouping of PFAS may not be sufficient to predict their biological effects. Testing of individual PFAS may be needed for scientific-based decision-making. Our proposed strategy of

[$]Current address: Program in Molecular and Integrative Physiological Sciences, Department of Environmental Health, Harvard T.H. Chan School of Public Health, Boston, Massachusetts 02115, USA

Conflict of interest

The authors declare no conflicts of interest.

using two human cell types and considering phenotypic and transcriptomic effects, combined with dose-response analysis and calculation of BER, may be used for PFAS prioritization.

Keywords

perfluoroalkyl substances; iPSC; transcriptomic; chemical safety; high-throughput

Introduction

Per- and polyfluoroalkyl substances (PFAS) are man-made chemicals that contain carbon-fluorine bonds with distinct end functional groups (Carlson et al., 2022). The Organisation for Economic Co-operation and Development (OECD) maintains an inventory of PFAS that contains over 4,700 substances (OECD, 2018), albeit estimates exceeding 10,000 PFAS have also been reported (Williams et al., 2017). PFAS are widely used in industrial applications and consumer products and many of them are highly persistent, water soluble and mobile, leading to environmental dispersal and accumulation in the water, soil, wildlife, and ultimately humans.

While some PFAS, such as perfluorooctanoic acid (PFOA) and perfluorooctane sulfonic acid (PFOS), have been studied extensively and reports of their adverse health effects are abundant (Fenton et al., 2021; Meneguzzi et al., 2021), the vast majority of PFAS lack toxicity data. For example, a systematic evidence map of available epidemiological and animal bioassay evidence for a set of ~150 PFAS that were prioritized in 2019 by the U.S. EPA for *in vitro* toxicity and toxicokinetic testing showed that only 45 compounds had some data in either animal or epidemiology studies (Carlson et al., 2022). However, a growing body of evidence suggests that other PFAS may also pose human health hazards (National Toxicology Program, 2019a, b). Because of the growing concern about the persistence of PFAS and the potential that they may be hazardous to both human health and the environment, on 13 January 2023 health and environmental protection authorities in Denmark, Germany, the Netherlands, Norway and Sweden proposed restrictions on PFAS as a class (ECHA, 2023). Because of the considerable data gaps on virtually all PFAS, there is a significant need for and interest in accelerating the process of generating toxicology and exposure data that will inform decision-making.

One of the key needs in PFAS risk assessment is a scientifically-supported strategy for prioritization of PFAS for testing. In both the United States and Europe, regulatory bodies proposed a pragmatic approach of grouping PFAS into categories followed by selection of representative compounds for further study (ECHA, 2023; U.S. EPA, 2021). A common approach is to group PFAS based on structural similarities (Buck et al., 2011; Sha et al., 2019; Wang et al., 2017; OECD, 2018). This approach has been applied to define groups of PFAS for risk assessment (Patlewicz et al., 2019; Buck et al., 2021). For example, the US EPA has established a workflow for PFAS evaluation that prioritized a subset of compounds to maximize information to support read-across within structure-based groupings (Patlewicz et al., 2019; Carlson et al., 2022).

The canonical read-across approach assumes that the chemical's toxicological properties can be inferred from those of a structurally similar chemical (Ball et al., 2016). Structure-property relationships are used to estimate the bioaccumulation potential of novel and emerging PFAS, as well as their protein binding and elimination rates (Cousins et al., 2020; Cheng and Ng, 2018; Gomis et al., 2018). The structure-property relationships have been reported for human hepatocyte lipid accumulation and gene expression in a study of 19 PFAS (Marques et al., 2022). Read-across approaches are already applied for PFAS management; for example, the State of Massachusetts proposed maximum contaminant level values for drinking water based on similarities in chemical structure and effects (Massachusetts Government, 2020). Still, questions remain whether grouping of PFAS based on structure alone is scientifically justifiable.

Additional data, including that from *in vitro* studies, may provide a biological dimension for informing class-based approaches for read-across and/or within-group prioritization for additional testing. Indeed, toxicity and toxicokinetic data are being generated using *in vitro* testing and computational methodologies to inform PFAS hazard characterization (US EPA, 2019; Patlewicz et al., 2019; Kreutz et al., 2023; Dawson et al., 2023; Patlewicz et al., 2022; Carstens et al., 2023). In addition, gene expression data offer a comprehensive understanding of chemical-induced bioactivity, delivering not only mechanistic insights but also dose-response information (Reardon et al., 2023; Johnson et al., 2022). Several studies have tested effects of PFAS on gene expression in human liver spheroids and demonstrated that both mechanistic insights and dose-response information can be used for ranking/prioritization and comparison to the effects in rodent liver (Rowan-Carroll et al., 2021; Reardon et al., 2021).

Based on the regulatory need to group PFAS and previous studies demonstrating the value of *in vitro* studies for dose-response analysis, we tested 26 PFAS from 8 structurally diverse groups in two human cell types from organs that are known to be targets for PFAS. We evaluated a hypothesis that structure-based grouping of PFAS can be substantiated using *in vitro* bioactivity data from both phenotypic and transcriptomic endpoints, and that these data may be also used for risk-based prioritization of PFAS. To address this hypothesis, we tested concentration-response effects on both cell function and gene expression in human induced pluripotent stem cell (iPSC)-derived hepatocytes and cardiomyocytes. The selection of these two cell types was informed by current knowledge and research gaps. Liver toxicity is one of the most studied effects of PFAS exposure (National Academies of Sciences Engineering and Medicine, 2022). Additionally, the potential cardiotoxic effects of PFAS exposure are currently understudied (National Academies of Sciences Engineering and Medicine, 2022), underlining the need for further investigation using *in vitro* models (Burnett et al., 2021a). Phenotypic and transcriptomic points of departure were derived to quantify the bioactivity of tested PFAS, and a transcriptomic pathway enrichment analysis was performed to determine potential similarities in the molecular effects of substances within and between chemical classes. Finally, the transcriptomic and phenotypic PODs were compared to exposure data to derive bioactivity-to-exposure ratios (BER).

Materials and Methods

Chemicals and Biologicals

Test PFAS (n = 26, Tab. 1) were obtained from the United States National Toxicology Program as 20 mM stocks in 100% tissue culture grade dimethyl sulfoxide (DMSO). The PFAS were selected based on preliminary bioactivity data, from which high and low rank chemicals were then selected in a smaller subset of PFAS with diverse structures for additional *in vitro* screenings. The PFAS were assigned into sub-categories using the head-group/side-chains to determine their classification as previously suggested (OECD, 2018; Buck et al., 2011; Buck et al., 2021). Tested PFAS, abbreviations, and their chemical structure-based category information are listed in Tab. 1. Tissue-culture grade DMSO (CAS# 67–68-5, sc-358801) was used as the vehicle for all studies and was obtained from Santa Cruz Biotechnology (Dallas, TX, USA).

Cell-specific positive controls were used for both the iPSC-derived hepatocytes (iPSC-Hep) and cardiomyocytes (iPSC-CM). The positive controls for the iPSC-Hep were rotenone (CAS# 83–79-4, Cat# 45656–250MG), amiodarone (CAS# 19774–82-4, Cat# A8423–1G), acetaminophen (CAS# 103–90-2, Cat# A5000–100G), and CCCP (carbonyl cyanide 3-chlorophenylhydrazone, CAS# 555–60-2, Cat# C2759–100MG); all were purchased from Sigma-Aldrich (St. Louis, MO, USA). Isoproterenol, sotalol, and propranolol (Molecular Devices, San Jose, CA, USA) were used as the positive controls for the iPSC-CM. Tetra-octyl ammonium bromide (TAB, CAS#14866–33-2, Cat# D2438) was obtained from Sigma-Aldrich (St. Louis, MO, USA) and used as a positive control for both cell types.

Human iPSC-Hep and iPSC-CM cells were obtained from FUJIFILM Cellular Dynamics (Cat# C1023 and Cat# C1006, respectively; Madison, WI, USA), along with their corresponding plating and maintenance media. Additional reagents including RPMI medium (Cat# 11875–093), dexamethasone (Cat# A13449), B27 supplement (Cat# 17504–044), gentamicin (Cat# 15750–060), and penicillin-streptomycin (Cat# 15140–122) were obtained from Gibco (Waltham, MA, USA). Oncostatin-M was from R&D Systems (Cat# 295-OM-010, Minneapolis, MN, USA).

For cell culture, we used tissue-culture-grade 384-well plates (for iPSC-CM, Cat# 3764, Corning Life Sciences, Kennebunk, ME, USA) and collagen I pre-coated 384-well plates (for iPSC-Hep, Cat# 354664, Corning Life Sciences). Other reagents included gelatin (Cat# G1890–500G), Trypan Blue 0.4% solution (Cat# T8154–100ML), and D-PBS (Cat# D8537) were obtained from obtained from Sigma-Aldrich.

Cell Culture

Cells were plated and maintained in tissue culture-treated 384-well plates according to instructions provided by FUJIFILM Cellular Dynamics and as described previously (Sirenko et al., 2014; Grimm et al., 2015). Briefly, iPSC-Hep were thawed for 3 min in a water bath at 37°C. The thawed cells were then transferred to a 15 mL tube, 9 mL of plating media was then added. The plating media contained RPMI medium with 2% (v/v) of iCell Hepatocyte Medium Supplement, 0.1 μM of dexamethasone, 2% (v/v) of B27 supplement, 25 μg/mL of gentamicin, and 20 ng/mL of Oncostatin-M. The cells were then counted using an automated

cell counter and subsequently diluted to reach the final cell density of 7.2×10^5 cells/mL. The cell suspension was then transferred to collagen I pre-coated 384-well plates, yielding a final seeding density of 18,000 cells/well. Cells were plated in the inside wells (a total of 308-wells) and the outer-wells were filled with PBS to help insulate the inner wells and avoid evaporation. Plates were kept at room temperature for 30 min before they were placed in the incubators at 37°C and 5% CO_2. Four hours post-plating, the plating medium was exchanged with 25 μL of fresh plating medium. Thereafter, the plating medium was exchanged daily until day 5 post-plating. On day 5, the plating medium was exchanged with maintenance medium made from RPMI medium containing 2% (v/v) of iCell Hepatocyte Medium Supplement, 0.1 μM of dexamethasone, 2% (v/v) of B27 supplement, 25 μg/mL of gentamicin, and 20 ng/mL of Oncostatin-M; this medium was used for the remainder of the experiment and replaced every other day until the chemical exposure on day 7.

For experiments in iPSC-CM, plates were prepared by adding 25 μL of 0.1% (w/v) gelatin solution per well and incubated for 2 h at 37°C and 5% CO_2. Vials containing iPSC-CM were thawed for 3 min in a water bath at 37°C. The contents of a single vial were then added to a 15 mL conical tube and an additional 9 mL of plating medium containing 1:500 (v/v) penicillin/streptomycin solution was added. An aliquot of the cell suspension was used to count the cells, further dilutions were done if necessary to yield the target viable cell seeding density of 2×10^5 viable cells/mL. Immediately, before plating, the gelatin solution was fully aspirated from the plates and 25 μL of cell suspension was added to each of the 308 wells, resulting in an estimated cell density of 5,000 viable cells/well. The outer wells were filled with PBS to help insulate the wells and avoid evaporation. Plates were kept at room temperature in the hood for 30 min and then placed in the incubator at 37°C and 5% CO_2. Forty-eight hours after cell seeding, the plating medium was exchanged by removing 17.5 μL/well and replacing it with 32.5 μL of maintenance medium containing 1:500 penicillin/streptomycin. Maintenance medium was subsequently changed every other day for the remaining 12 days in culture until the chemical exposure and assays. On the evening before chemical addition, the medium was removed and replaced by 25 μL of fresh maintenance medium.

To evaluate the functional and cytotoxic phenotypes in iPSC-Hep, they were exposed to the PFAS for 48 hours for the functional, cytotoxic, and genomic endpoints. The iPSC-CM were exposed to the PFAS for 90 minutes and for 24 hours for the gene expression studies. For the functional and cytotoxic phenotypes, various stains and images were collected at the respected timepoints as detailed below, and for the genomic endpoints cell lysates were collected at the respective timepoints for transcriptomic analyses.

Plate Design

A 200× chemical master plate was first prepared in 100% cell culture-grade DMSO, the chemicals were then transferred to the 5× working plate (2.5% DMSO and 97.5% cell-specific culture medium). For the final assays (1×), 12.5 μL of the solutions in the working plate were added to the assay plate that contained cells in 50 μL of cell-specific medium, yielding a final concentration of 0.5% DMSO. Each assay plate contained 308 wells with cells and (i) each chemical ($n = 26$) and concentration (PFAS were tested in 4

final concentrations of 0.1, 1, 10, and 100 μM), (ii) vehicle (DMSO at final concentration of 0.5%) wells (n = 14), (iii) media-only wells (n = 6), and (iv) wells with cell type-specific positive controls (n = 20). The entire chemical layout was repeated twice per 384-well plate. The top tested concentration (100 μM) was not used for the genomic assays.

Phenotype Assays

On day 7 post-plating, iPSC-Hep were exposed to test chemicals for 48 hours. Chemical transfer from the master plate (200×) to the working plate (5×) and then to the assay plate (1×) was done using automated liquid handling of the FLIPR Tetra (Molecular Devices, San Jose, CA). After a 48-hour exposure at 37°C and 5% CO_2, the medium was replaced with medium containing fluorescent dyes—MitoTracker, Hoechst 33342, and Calcein AM—to assess mitochondrial, nuclear, and cytoplasmic endpoints. Following a 15-minute incubation at 37°C, the medium with dyes was replaced with fresh maintenance medium. The plates were then transferred to the ImageXpress Micro Confocal High-Content imaging system (Molecular Devices) for image analysis. Data for functional and cytotoxic endpoints was extracted using MetaXpress Software Multiwavelength Cell Scoring Module (Molecular Devices).

On day 14 post-plating, for the iPSC-CM, Ca^{2+} flux was measured before and after chemical exposure using the EarlyTox Cardiotoxicity Kit (Molecular Devices) as detailed in (Grimm et al., 2015). First, the Ca^{2+} dye reagent (25 μL) was added to each well and incubated at 37°C for 2 hours. A baseline read was recorded using the FLIPR Tetra. Chemicals were then immediately added from the working plate (5×), transferring 12.5 μL to the assay plate (1×) (total volume of 62.5 μL) using the automated liquid handling of the FLIPR Tetra from the 5× working plate, the plates were then incubated for 90 minutes at 37°C. The Ca^{2+} flux was measured again, and the medium with chemicals was then replaced with the medium containing fluorescent dyes, specifically MitoTracker (2 μg/mL) and Hoechst 33342 (200 nM). After a 15-minute incubation with the fluorescent probes, the medium was replaced with fresh maintenance medium and the plates were transferred to the ImageXpress Micro Confocal High-Content imaging system (Molecular Devices) for image acquisition. The imaging data were subsequently analyzed using the MultiWavelength Cell Scoring Module available on the MetaXpress software and the data from relevant endpoints were extracted using both MetaXpress Software on the ImageXpress Micro Confocal High-Content Imaging System for cytotoxic endpoints and Screenworks 4.0 software on the FLIPR Tetra for the functional endpoints (Molecular Devices). The raw data for both cell types and all phenotypes are available as Supplementary Files 1 and 2.

Derivation of the Phenotypic Points of Departure (pPODs)

For pPOD derivation, first, normalization of phenotypic readouts to their respective vehicle (0.5% DMSO) controls was conducted. The vehicle-treated (0.5% DMSO) samples were then screened to identify any outliers (measurements falling outside of the inter-quartile range), and outliers were removed if present. Vehicle control-scaled data for each test substance and phenotype were then fitted to a curve with a nonlinear logistic (Hill) function to determine POD values (Sirenko et al., 2017), defined as the concentrations at which the fitted curve exceeds certain thresholds above or below the mean of vehicle-treated controls

(benchmark responses for each phenotype are detailed in Tab. 2). For iPSC-Hep, the choice of one standard deviation “benchmark response” was based on US EPA guidance (Wignall et al., 2014) and empirical observations that generates consistently high classification accuracy (Sirenko et al., 2017). For iPSC-CM, the POD values were derived based on the criteria consistent with human clinical cardiotoxicity phenotypes as previously described (Blanchette et al., 2020).

TempO-Seq Library Preparation and Sequencing

Following chemical exposure, the wells were completely aspirated and 10 μL/well of 2× lysis buffer (BioSpyder Technologies, Carlsbad, CA) was added to each well and plates were placed on an orbital plate shaker at room temperature for 10 minute to facilitate cell lysis. Then, adhesive seals were placed on the plates and the lysates were frozen in the 384-well plates and stored at −80°C until further processing. The Templated Oligonucleotide Sequencing Assay (TempO-Seq™, BioSpyder Technologies) was used as the RNA sequencing technology and gene expression was evaluated using the human TempO-Seq Whole Transcriptome panel (BioSpyder Technologies) consisting of 22,537 protein-coding probes. Detailed protocols for TempO-seq are provided by the manufacturer and have been previously reported elsewhere (Grimm et al., 2016; House et al., 2017). Briefly, an aliquot (2 μL) of the cell lysate was transferred to a 96-well plate, in which the samples first underwent annealing to match detector oligos, followed by nuclease digestion of excess oligos, detector oligo ligation, which are subsequently amplified with the tagged primers according to manufacturer instructions (BioSpyder Technologies). The amplified samples were then pooled and purified into a sequencing library using a PCR clean-up kit (Clontech, Mountain View, CA). The libraries were sequenced (single-end, 50 bp in length) using HiSeq 2500 v.2 (Illumina, San Diego, CA). The reads were then aligned to target probe sequences to generate a gene count matrix using the analysis pipeline detailed elsewhere (House et al., 2017) including the STAR aligner (Dobin et al., 2013) with the maximum number of allowed mismatches of 3, insertion/deletion open, and extension penalty of 0.

Gene Expression Data Analysis

Probe read count data for transcripts with more than one probe in the TempO-Seq assay was first summed to gene level. Quality control steps with the following criteria were performed: 1) genes with fewer than 5 mean counts across the entire sample space ($n = 330$ for iPSC-Hep and $n = 220$ for iPSC-CM) were removed, 2) samples with mean expression across all genes lower than 25 were removed, 3) outliers in vehicle control samples were identified and removed using mean correlation at <0.85 as the criteria to ensure the stability of further transcriptomic dose-response and differential expression analyses, 4) in addition, principal component analysis (PCA) was conducted on vehicle control samples using raw counts to identify any remaining outliers. After these quality control steps, 330 samples and 10,205 genes were retained for further analyses in iPSC-Hep, and 202 samples and 15,112 genes in iPSC-CM.

Bioconductor’s DESeq2 package (Love et al., 2014) was used to perform differential gene expression analysis and to rank genes based on the $\log_2$-fold-change values by contrasting

the samples from the highest tested concentration (10 μM) of each PFAS substance and the vehicle controls. The ranked genes were then analyzed using Gene Set Enrichment Analysis (GSEA) approach (Subramanian et al., 2005) to derive enriched Reactome pathways (Jassal et al., 2020) as implemented in the gsePathway functions of R package ReactomePA version 1.16.2 (Yu and He, 2016). To enhance the interpretability, an additional data integration step was implemented to group significantly enriched gene sets from lower-level pathways into common higher-level nodes based on the REACTOME pathway hierarchy (Jassal et al., 2020).

Analysis of variance (ANOVA) for categorical effects on individual genes was performed using the aov command in R. For those genes that were significant (FDR q-value< 0.05), a two-tailed post-hoc Tukey test was conducted using the TukeyHSD command in R as a guide to describe the categorical gene expression effects between individual PFAS sub-groups.

Supervised Category Analysis Using Prediction Analysis of Microarrays

A machine-learning statistical model was trained to predict the structure-based PFAS categories using the Prediction Analysis of Microarrays (PAM) approach. The approach performs class prediction via nearest shrunken centroid for a high-dimensional vector and works for any quantitative set of features. The analysis utilized gene expression log-2-fold-change profiles as predictors, along with bioassay measurements (phenotypic PODs) in both cell types, performed using pamr version 1.56.1 (Tibshirani and Efron, 2002). PFAS categorical predictions were made using expression data alone and phenotypic PODs alone in each cell type, as well as a combination of expression data and phenotypic PODs in both cell types. For this analysis the FTCA “group” with only one PFAS member was removed, as it is not suitable for cross-validation. The cross-validated matching accuracy, derived from the associated confusion matrix, was computed to show the proportion of matches between predicted category assignments using training data only, and true assignments. The proportion of matches expected under chance was determined by 1 million random permutations of group assignments, with a mean of 0.21 and 95^{th} percentile of 0.32. Thus, a cross-validated matching prediction proportion in excess of 0.32 would be considered significant at the 0.05 level.

Transcriptomic Benchmark Dose Modelling and Derivation of the Transcriptomic Points of Departure (tPODs)

The Bioconductor’s DESeq2 package (Love et al., 2014) was utilized to assemble the complete normalized count matrix as detailed above. The normalized counts data (counts + 1 to zero-protect the data for further analyses on the logarithmic scale) were processed using the BMDExpress (v.2.3) software (Phillips et al., 2019) for transcriptomic benchmark dose modelling as detailed in (Tsai et al., 2023). Data were first pre-filtered with Williams’ trend test (p-value ≤0.05 within each transcript and substance) and an absolute fold change ≥1.5 (compared with vehicle controls); genes that did not pass these criteria at any dose were removed from further analysis. Next, data were analyzed using Hill (version 2.18), power (version 2.19), linear (version 2.21), polynomial 2 (version 2.21), and exponential (2, 3, 4, and 5, version 1.11) models. A benchmark response of 1 standard deviation was used at

the individual gene level to derive a benchmark dose (BMD). The best-fit model for each transcript was selected based on the following parameters: (1) maximum iterations of 250; (2) confidence level of 0.95; (3) constant variance; Hill models with a k parameter <1/3 of the lowest positive dose were flagged and then the next best model with a p-value >.05 was used; and (5) a nested chi-squared cutoff value of 0.05 to select the best polynomial models followed by minimum Akaike Information Criterion value and a goodness-of-fit p-value >0.05. The BMD output data files from BMDExpress are available as Supplementary Files 3 and 4.

Transcripts that had BMD upper bound (BMDU) to BMD lower bound (BMDL) ratio >40 or a model fit p-value <0.1were excluded from further analyses. Vehicle control samples were assigned a “dose” one $\log_{10}$ unit below the lowest dose tested to allow plotting on the logarithmic scale, as well as allowing capping the BMD values at the lowest dose tested. In addition, BMD values were also capped at the highest dose tested.

For derivation of tPOD for each tested substance, the lowest gene set median gene BMD was used based on features that passed the criteria described above in accordance with previously published guidance (National Toxicology Program, 2018). Gene sets were represented by both enriched pathways (Reactome and KEGG annotations) and Gene Ontology (GO) biological process and were identified using xgr package version 1.1.8 in R (Fang et al., 2016). The gene set background list included all interrogated genes retained after low count removal. Subsequently, the lowest median BMD value from any gene set was selected as the tPOD for each tested PFAS and cell type.

Selection of CRGs that were Common Across Multiple PFAS

To assess whether different PFAS had similar concentration-response effects at the gene level, we employed permutation-based significance testing. Specifically, for each cell type separately, the binary recorded matrix was established, with individual CRGs as rows and PFAS as columns, where 0 indicated no significant concentration-response for each gene-PFAS pair, and 1 indicated that a PFAS elicited concentration-response of a transcript. Then, the data matrix was permuted column-wise, shuffling the elements of each column randomly. For each permutation iteration, the sum of each row (instances of a gene declared as CRG) across all PFAS was calculated. This process was repeated 10,000 times to construct a null distribution for each gene. The row sums from each permutation were stored for each iteration. The empirical p-value for each gene was then computed by comparing the observed sum for each gene (data from the actual experiment) to the null distribution. Genes with empirical p-values < 0.05 were considered statistically significant.

Derivation of the Bioactivity-to-Exposure Ratios (BER)

To compare the bioactivity derived from *in vitro* assays and exposure levels, *in vitro*–to–*in vivo* extrapolation was performed using the equation detailed below (Eq. 1) to convert exposure dose level (mg/kg/day) to μM units. The equation was adopted from (Wetmore et al., 2012), where the original format was to convert an *in vitro* bioactivity value (μM) to an oral equivalent dose (mg/kg/day).

$$Exposure\ \ estimates\ \ (\mu\mathrm{M}) = \frac{95th\ \ percentile\ \ exposure\ \ prediction\ \ (mg/kg/day) \times Css\ \ (\mu\mathrm{M})}{1\ \ (mg/kg/day)}$$

(Eq. 1)

This conversion used either human steady-state plasma concentrations (Css) from the httk R package (Pearce et al., 2017); or the predicted fraction unbound data from recent publications (Kreutz et al., 2023; Smeltz et al., 2023). See Css and exposure values for 18 PFAS that had available data from either source in Tab. S1. To ensure consistency and conservative assumptions when integrating Css data from various sources, intrinsic clearance was set to zero during the derivation of Css values. The BERs (Paul Friedman et al., 2020) were computed by dividing POD values from the *in vitro* experiments (this study, μM) by the 95th percentile exposure predictions (μM, as calculated using Eq. 1) for the general U.S. population, as derived from the ExpoCast Systematic Empirical Evaluation of Models version 3 (SEEM3) framework (Ring et al., 2019). The equation for BER calculation was detailed below (Eq. 2)

$$Bioactivity - to - Exposure\ \ Ratios\ \ (BER) = \frac{Points\ \ of\ \ departure\ \ (\mu\mathrm{M})}{Exposure\ \ estimates\ \ (\mu\mathrm{M})}$$

(Eq. 2)

Results

This study tested a hypothesis that structure-based grouping of PFAS can be substantiated using *in vitro* bioactivity data from both phenotypic and transcriptomic endpoints, and that these data may be used for risk-based prioritization of PFAS. The study's overall design and data analysis workflow are depicted in Fig. 1. Specifically, we evaluated 26 PFAS (Tab. 1) that belong to 8 sub-groups based on established nomenclature (OECD, 2018; Buck et al., 2011; Buck et al., 2021). Bioactivity of PFAS compounds was tested using iPSC-hepatocytes (iPSC-Hep) and iPSC-cardiomyocytes (iPSC-CM), cells selected to be representative of organs of concern for potential adverse effects of PFAS (National Academies of Sciences Engineering and Medicine, 2022). Both phenotypic and transcriptomic data were analyzed to identify points of departure (PODs) and potential underlying mechanisms of PFAS effects. For risk characterization, we calculated bioactivity-to-exposure ratios (BERs) using conservative exposure estimates and the lowest POD.

Phenotypic Effects of PFAS in iPSC-Hep and iPSC-CM

PFAS compounds (Tab. 1) were tested in iPSC-Hep and iPSC-CM in concentration response (0.1, 1, 10, and 100 μM) and both functional and cytotoxicity phenotypes were evaluated (Tab. 2). Fluorescent imaging of the cytoplasm, nuclei and mitochondria were used as relevant phenotypes in iPSC-Hep (Grimm et al., 2015; Sirenko et al., 2014). In iPSC-CM, Ca^{2+} flux was used as the primary indicator of the ion channel activity and beat frequency (Sirenko et al., 2017; Sirenko et al., 2013). Fig. 2A shows representative Ca^{2+} flux traces for iPSC-CM that were treated with vehicle (spontaneous frequency of ~30 beats per minute) or two representative PFAS that elicited negative chronotropy effects at the highest

concentration tested (100 μM) – perfluorobutanesulfonic acid (PFBS, 24 beats per minute) and perfluorotridecanoic acid (PFTiDA, 12 beats per minute). Dose-response modeling was performed on the data from each phenotype and PODs were derived using phenotype-specific benchmark responses as indicated in Tab. 2.

Fig. 2B depicts a heatmap of phenotypic PODs (pPOD) for each individual PFAS in both iPSC-Hep and iPSC-CM. In this supervised analysis, PFAS were arranged by their respective chemical structure group (Tab. 2), by cell type and phenotype. In iPSC-Hep, only two PFAS elicited concentration-response phenotypic effects – PFOA and PFHx2Et2OA; both compounds increased mean cell area which is indicative of cell enlargement most likely due to fatty accumulation. In iPSC-CM, 8 PFAS elicited effects that reached a benchmark response (Tab. 2) for two phenotypes – decreased peak frequency (PFBS, PFDS-Na, 8:2 FTS, PFOA, PFTeDA, PFTiDA, NH4PFOA, and PFMPA), and QT prolongation (PFDS-Na). No patterns in phenotypic effects of tested PFAS in either cell type were evident with respect to PFAS chemical structure-based classes except for negative chronotrope, where by there were relatively higher number of substances in PFCA and PFSA groups with effects; however, one-way ANOVA showed no significant difference among classes ($p = 0.22$). In addition, no significant correlation was found between pPOD and either chain length (Spearman $\rho = -0.15$, $p = 0.50$ in iPSC-CM; $\rho = -0.02$, $p = 0.94$ in iPSC-Hep) or molecular weight ($\rho = -0.29$, $p = 0.15$ in iPSC-CM; $\rho = 0.06$, $p = 0.76$ in iPSC-Hep) for the tested PFAS.

Transcriptomic Effects of PFAS in iPSC-Hep and iPSC-CM

While few concentration-response phenotypic effects were observed at the whole cell level, gene expression was evaluated to determine whether PFAS had molecular-level effects in both iPSC-Hep and iPSC-CM. These analyses (Fig. 1) included (i) determination of the effects at gene and pathway level at the highest concentration tested for gene expression analysis (10 μM), (ii) analysis of the concentration-response at the gene level (vehicle, 0.1, 1 and 10 μM), and (iii) derivation of the transcriptomic PODs at the pathway/gene set level (tPODs).

First, we used raw gene expression data for each PFAS (10 μM) to conduct a principal components analysis (PCA). When all samples (PFAS and vehicle, in both cell types) were included in the PCA analysis (Fig. S1), the greatest separation was observed between cell types, as expected. While vehicle-treated samples were most distinguishable from PFAS-treated ones in iPSC-Hep, some compounds exhibited effects in both cell types. Therefore, differential gene expression was analyzed separately by cell type and compared to vehicle-treated samples. Two PCAs are shown in Fig. 3 to visualize such analyses for each cell type. Individual PFAS were colored by their chemical structure-based class (Tab. 1). This analysis showed that differential gene expression effects of PFAS exhibited little grouping by their chemical structure-based class in both cell types. To further investigate the grouping effects from gene expression data, ANOVA analyses were performed on log-2-fold-change values for individual genes derived from comparing the highest concentration and control samples. Only a very few genes (9 out of 10,205) in iPSC-Hep were found to be exhibit significant differences across the groups, whereas no gene showed significance in iPSC-CM.

The results indicate minimal effects on expression corresponding to the structure-based categories in both iPSC-Hep and iPSC-CM. The list of genes and the between-group comparisons that passed the post-hoc Tukey tests are presented in Supplementary File 5. Furthermore, to directly assess the potential correspondence of multiple features in gene expression and phenotypic bioactivity data to the structure-based groups, the PAM approach (see Methods) was used to fit a machine-learning model for PFAS categorical predictions (Supplementary Figures 2 and 3). However, the prediction accuracy was not significant across all data types tested: transcriptomic data, phenotypic POD data, and a combination of both.

Second, as a surrogate measure of the potency of the tested PFAS' effect on transcription, we evaluated concentration-response for each compound by determining the number of concentration responsive genes (CRGs) in each cell type (Fig. 4). Higher counts of CRGs may be interpreted as greater bioactivity. In iPSC-Hep, the number of CRGs affected by PFAS ranged from 116 (representing 1.1% of the total number of expressed genes in this cell type) to 542 (5.3%). In iPSC-CM, the numbers of PFAS-effected CRGs varied more widely, from 83 (0.5% of the total number of expressed genes in this cell type) to 2,027 (13.4%). The bar plots in Fig. 4 show that the number of CRGs for individual PFAS were substance- and the cell type-specific and not dependent on their chemical structure-based class ($p = 0.26$ in iPSC-Hep; $p = 0.75$ in iPSC-CM using one-way ANOVA). No significant correlation was found between the number of CRGs and either chain length ($\rho = -0.08$ in iPSC-CM; $\rho = 0.14$ in iPSC-Hep) or molecular weight ($\rho = -0.17$ in iPSC-CM; $\rho = 0.17$ in iPSC-Hep) for tested PFAS.

Third, we examined whether there were similarities in CRGs among PFAS. For this, we employed permutation-based significance testing to determine whether some genes were concentration-responsive across multiple PFAS, beyond chance variation expected when comparing thousands of genes. An empirical p-value was calculated by permutation analysis. Fig. 5 shows the top 50 genes that were most frequently concentration-responsive (either up- or down-regulated) to PFAS in each cell type. In this figure, genes are ranked by the frequency of them being identified as a significant CRG in response to PFAS treatment. Almost all the transcripts identified in this analysis were upregulated in response to PFAS and they were also highly cell-type specific. Only one transcript, *ADAMTS9*, encoding disintegrin and metalloproteinase with thrombospondin motifs, a gene that is expressed ubiquitously in multiple cell types, was significantly concentration-responsive to PFAS treatment in both iPSC-Hep and iPSC-CM. Genes known to play a role in xenobiotic metabolism or muscle contraction pathways were among the top 50 CRGs in iPSC-Hep or iPSC-CM, respectively. While many of the effected genes were shared among PFAS in each cell type, no gene was shared among more than half of tested compounds. The gene in highest commonly shared frequency – *CDH6* in iPSC-Hep and *NDUFA10* in iPSC-CM – was significant in concentration-responsive effects in 10 (38%) and 9 (35%) of tested PFAS, respectively. Still, depending on the gene, anywhere from ~25% to ~40% of the tested PFAS shared common concentration-response effects on gene expression. It is also noteworthy that almost all the shared CRGs in both cell types were showing upward concentration response trends.

Fourth, because we observed that common individual CRGs are known to be involved in the mechanisms of hepato- (Rusyn et al., 2021) and cardio- (Lind et al., 2021) toxicity, we aimed to investigate shared pathway-based effects of PFAS and whether these effects are dependent on their chemical structure-based class. For this, we employed the Gene Set Enrichment Analysis approach (Subramanian et al., 2005) to overcome the limitations associated with the utilization of arbitrary thresholds during the selection of significant differentially expressed genes. This method involves evaluation of cumulative changes in gene expression across entire sets of genes, rather than focusing on specific genes that exceed a predetermined significance threshold. To execute this analysis, we utilized ranked $\log_2$-fold change values obtained by comparing expression levels of each gene at the highest concentration tested with that in vehicle controls. A complete list of gene sets that were significant is included in Supplementary Files 6 and 7, and the corresponding heatmaps using the data were included in Supplementary Figures 4 and 5. To enhance clarity and interpretability of the outcome of this analysis, an additional data integration step was undertaken to group significantly enriched gene sets from lower-level pathways into common higher-level nodes based on the REACTOME pathway hierarchy (Jassal et al., 2020). This organization allowed for a clearer depiction of the common mechanistic events that were affected by tested PFAS. Fig. 6 shows that as many as 25 and 18 (out of 26 tested) PFAS exhibited similarity in a number of pathway-level effects in iPSC-Hep and iPSC-CM, respectively. In iPSC-Hep, significantly enriched and upregulated pathways included extracellular matrix organization, translation, RNA and general metabolism, and cellular response to stress. Pathways for plasma lipoprotein assembly, remodeling, and clearance were consistently down-regulated in iPSC-Hep by the majority of tested PFAS. In iPSC-CM, all significant pathways were upregulated and the top effected one was related to muscle contraction, followed by several pathways that are related to energy supply, events that are required for efficient muscle contraction. We also examined whether chemical structure-based class-specific effects could be discernable at the pathway level in either cell type using heatmap to visualize the enriched pathways versus individual PFAS but found none (data not shown), indicating similarity in transcriptomic effects for PFAS as a class at the pathway level rather than the similarity in sub-group.

Fifth, we calculated transcriptomic PODs (tPODs) at the pathway/gene set level. Recent studies demonstrated the value of using transcriptomic data for dose-response analysis in addition to their traditional use for mechanistic interpretation (Farr and Dunn, 1999; Johnson et al., 2020; LaRocca et al., 2017; Vinken et al., 2017). We used the most sensitive pathway method to derive tPODs, a common approach to dose-response modeling in transcriptomic datasets (National Toxicology Program, 2018). For each substance, the tPOD is a benchmark dose of the median gene in the most sensitive pathway/gene set effected by PFAS treatment (see Methods). Fig. 7 shows a comparison between tPODs and numbers of CRGs for each PFAS and cell type. A wide range in tPODs was observed among PFAS in each cell type. In iPSC-Hep, only 3 (12%) of 26 tested PFAS had no tPOD, and 23 PFAS had tPOD <10 μM. A significant negative correlation was observed between tPODs and the number of CRGs in iPSC-Hep – as the number of CRGs increased, the tPODs value decreased (correlation coefficient, $r = -0.5$, p-value < 0.01). In iPSC-CM, 10 (38%) of 26 tested PFAS were without tPOD, and 16 PFAS had tPOD < 10 μM. No correlation was

found between tPODs and CRGs. In both cell types, tPODs were not clustering by their chemical structure-based class. No significant correlation was found between the tPODs and either chain length ($\rho = -0.16$ in iPSC-CM; $\rho = 0.003$ in iPSC-Hep) or molecular weight ($\rho = -0.06$ in iPSC-CM; $\rho = -0.05$ in iPSC-Hep) for tested PFAS.

Risk Characterization and Prioritization of PFAS Using In Vitro PODs

The analyses presented above showed that the hypothesis that structure-based grouping of PFAS can be substantiated using *in vitro* bioactivity data from both phenotypic and transcriptomic endpoints was not confirmed with the data from cell types we tested. However, *in vitro* data collected in these studies did show that PFAS elicit both phenotypic and transcriptomic bioactivity. Therefore, we reason that these data may be used for risk-based prioritization of PFAS. One approach is to prioritize PFAS for further testing using either phenotypic or transcriptomic PODs alone – the "protective" approach (Woodruff et al., 2023). The other is to combine the "protective" bioactivity-derived PODs and conservative exposure predictions to derive chemical-specific BERs (Paul Friedman et al., 2020). Fig. 8 presents both considerations as possible means for prioritization and risk characterization of PFAS. Fig. 8A plots the minimum (most protective) pPODs and tPODs for each tested PFAS separately for each cell type. The transcriptomics-based PODs were more sensitive (i.e., protective) overall to treatment with PFAS. Specifically, tPODs were lower than pPODs not only on average across all 26 tested PFAS, but also for 25 and 21 compounds in iPSC-Hep and iPSC-CM, respectively.

Next, the overall minimum POD for each substance (either tPOD or pPOD, from either cell type) was used to calculate the BERs (Fig. 8B). We used 95^{th} percentile of the exposure estimates from ExpoCast (Wambaugh et al., 2013), where available, for each PFAS; these were converted to concentrations as detailed in Methods. Data for both bioactivity and exposure predictions were available for 18 out of 26 PFAS; therefore, only these substances are included in Fig. 8B. Only 3 PFAS exhibited BERs lower than 1 (PFBS, 8:2 FTS and NH4PFOA); most substances ranged between 1 and 100. This suggests that when most conservative parameters are used for both bioactivity and exposure, several PFAS compounds could be identified as of potentially high concern and may warrant additional studies to refine estimates of both human health hazard and exposure.

Discussion

Grouping and read-across are widely used approaches, albeit to a varying degree of success, in evaluation of hazards and risks of chemicals that have data gaps (Ball et al., 2016). These approaches are pragmatic means to address the daunting task of evaluating PFAS, an overwhelming majority of which have no data to inform traditional hazard and risk evaluations. One commonly invoked grouping strategy for PFAS involves prioritization based on chemical structure features, which are believed to be most important in determining both toxicokinetic and bioactivity properties (Buck et al., 2011; Sha et al., 2019; Wang et al., 2017; OECD, 2018; Patlewicz et al., 2019; Buck et al., 2021). In this context, our study aimed to use both transcriptomic and phenotypic data from two human-health relevant (in terms of organs with known or potential PFAS hazardous effects) organotypic

(in terms their functionality) *in vitro* cell models to evaluate the association between structural groupings and bioactivity. In addition, regardless of whether structure-based grouping could be substantiated, we evaluated whether concentration-response analysis from both the transcriptomic and phenotypic data, combined with exposure estimates, may offer a sensible approach for risk-based prioritization of PFAS for additional exposure and hazard testing.

Relationship Between PFAS Structure-Base Classes and In Vitro Bioactivity

Several previous studies reported correlations between specific structural features of PFAS and their biological effects *in vitro.* For example, a study that examined effects of 142 PFAS in HepG2 cells (Houck et al., 2021) reported that PPAR activity correlated with physicochemical properties such as presence of the negatively charged structures and acidic hydrogen atoms; they also observed that RXRβ activation was associated with linear shapes and carboxylate groups. In another study of 15 PFAS (Zhang et al., 2014) the authors demonstrated that the binding affinity of PPAR gamma in HepG2 cells was linked to the chain length. Similarly, a study of 13 PFAS (Amstutz et al., 2022) found that increasing carbon chain length led to higher cytotoxicity in HepG2 cells. PFAS molecular weights were significantly correlated with protein binding association constants and contributed to lipid accumulation (Marques et al., 2022). In addition, a study of 147 PFAS identified a trend between molecular weight and bioactivity related to *in vitro* immunosuppression (Houck et al., 2023), and a study of 160 PFAS discovered that compounds with long carbon chains (8 or more carbons), high carbon to fluorine ratio, or containing a carboxylic acid moiety were more likely to exhibit developmental neurotoxicity *in vitro* (Carstens et al., 2023).

Still, little is known regarding structure-based group similarities in bioactivity even though the latter is a common hypothesis (Buck et al., 2011; OECD, 2018; Patlewicz et al., 2019; Buck et al., 2021). Our study examined potential associations between structural features detailed in previous studies and bioactivity in both iPSC-Hep. While we found few effects in iPSC-Hep, the most noteworthy observation with respect to whole cell bioactivity effects in our study comes from the data in iPSC-CM, a cell type that has not been studied with diverse PFAS previously. Our observation that 8 of 26 tested PFAS had effects on the beat frequency is novel and one that warranted additional mechanistic investigation using transcriptional data. Regardless of the cell type, however, we found little evidence of grouping similarity in the phenotypic effects. Moreover, in contrast to previous findings, our analysis also revealed no significant correlation between PFAS molecular weight or carbon chain lengths and bioactivity. The lack of significant correlations could be due to the number of PFAS used in this study or the cell types used. Further research using larger libraries of PFAS and additional cell types may be needed to confirm potential structure-activity relationships.

Mechanistic Similarity in the Transcriptomic Effects of PFAS

To further test whether molecular-level events may show evidence of similarity in biological responses to different PFAS, we used gene expression data. Indeed, demonstration of similar mode of action (MOA) has been suggested as a crucial consideration for attaining confident categorization/grouping of PFAS for human health risk assessment (Anderson et al., 2022).

Accordingly, we focused on the analysis of gene expression data in several ways, including concentration-response analysis and mechanistic interpretation. Previous studies of diverse PFAS in human hepatocytes or liver-derived cancer cell lines observed accumulation of intracellular lipids for several PFAS at concentration as low as 0.1 μM (Marques et al., 2022; Louisse et al., 2023). Similarly, gene expression studies in liver cells suggested that PFAS' structural features may be associated with lipid accumulation-related gene expression effects, including the relative potency of these effects (Reardon et al., 2021; Marques et al., 2022). These studies examined the relationships based on specific structural features, such as aliphatic chain length and molecular weight; they were not based on head group/side chain classification (OECD, 2018; Buck et al., 2011; Buck et al., 2021).

In our study, transcriptomic data in iPSC-derived hepatocytes confirmed the disruption of lipoprotein transport as the most prominent molecular event elicited by many of the tested PFAS. This observation aligns well with previous *in vivo* animal and epidemiological studies that established linkages between PFAS and alterations in serum lipoproteins and liver steatosis (Ho et al., 2022; David et al., 2023; Bijland et al., 2011). Indeed, a number of *in vivo* (Bijland et al., 2011; Curran et al., 2008; Das et al., 2017; Menger et al., 2020; Wan et al., 2012) and *in vitro* (Bjork et al., 2011; Hickey et al., 2009; Naile et al., 2012; Reardon et al., 2021; Rowan-Carroll et al., 2021) studies documented the disruptive impact of PFAS on lipid metabolism in the liver. Furthermore, gene expression data from iPSC-derived hepatocytes also suggested that PFAS may contribute to liver fibrosis, potentially via the upregulation of TGF-β. This finding is in support for the reported epidemiological and *in vitro* associations between fibrosis indicators and PFAS exposure (Cheng et al., 2023; Qi et al., 2023). However, our data show that these pathways were neither commonly enriched across all tested PFAS, nor was the significant enrichment associated with the chemical structure-based classes. It remains unclear whether the lack of an effect by some tested compounds was due to the tested concentrations being insufficient (highest concentration examined for gene expression was 10 μM), the choice of a liver cell type, or if some PFAS do not act on these pathways. *In vitro* models often require higher concentrations to demonstrate significant mechanistic results, whether in the case of human primary hepatocytes (Reardon et al., 2021; Rowan-Carroll et al., 2021; Marques et al., 2022; Robarts et al., 2022) or liver cancer cell lines (Solan and Lavado, 2023; Louisse et al., 2023; Robarts et al., 2022). Future research is needed to expand the range of tested PFAS, consider a broader spectrum of concentrations, and inclusion of more complex and physiologically-relevant liver model systems (Soldatow et al., 2013).

As we noted previously, published data on the possible associations between PFAS and cardiovascular adverse outcomes is less clear and not as abundant as that for liver. Some epidemiological studies showed the association between PFAS exposure and cardiovascular diseases (Meneguzzi et al., 2021); however, the evidence regarding associations between PFAS and overt cardiovascular disease remains limited and inconsistent (Schillemans et al., 2023). A better understanding of potential underlying molecular events in cardiomyocytes may help explain inconsistencies in epidemiological data; however, studies of heart-derived cells in toxicology are few (Burnett et al., 2021a). Mechanistic -omics and laboratory animal studies do indicate the potential for associations of some PFAS with multiple molecular pathways that could contribute to cardiovascular disease, but more information is needed

(Schillemans et al., 2023). For example, while some studies suggested that PFAS may affect developmental pathways during cardiomyocyte differentiation (Cheng et al., 2013; Davidsen et al., 2022; Davidsen et al., 2021; Tang et al., 2017; Zhang et al., 2016), few reports have been published to show effects on adult cells, especially of human origin, and a relatively small number of PFAS has been tested in human cardiomyocytes in culture (Burnett et al., 2021b).

In addition, while iPSC-derived cardiomyocytes are a useful model for cardiotoxicity screening, both in studies of cell function (Burnett et al., 2021a; Burnett et al., 2019; Chen et al., 2021; House et al., 2021) and in gene expression studies (House et al., 2022; Tsai et al., 2023; Grimm et al., 2018), gene expression effects from PFAS exposure in cardiomyocytes have not been reported. In this respect, our study provides a unique dataset that showed that PFAS exposure can perturb gene expression in iPSC-CM with patterns that were distinct from those in iPSC-Hep. Specifically, not only did we observe acute effects on the beat frequency, but we also observed that genes and pathways related to muscle contraction and energy supply were significantly affected, also in concentration-response manner (see below), by several PFAS. These findings suggest that further investigation is needed of PFAS-associated effects in human cardiomyocytes.

Using Transcriptomic Data for Concentration-Response Analysis

A number of studies in the past decade showed that the PODs derived from gene expression data in short-term animal studies are correlated with PODs from traditional apical (histopathology or clinical chemistry) endpoints in sub-chronic and chronic animal studies (Thomas et al., 2011; Johnson et al., 2020). More recently, gene expression data have been suggested to be of potential use to set accepTab. exposure limits for environmental chemicals – the US EPA has proposed to use transcriptomic reference values (TRV) as a novel EPA Transcriptomic Assessment Product (ETAP) (U.S. EPA, 2023). Therefore, transcriptomic data are not only regarded as useful in mechanistic interpretation, but also for dose-response step in risk assessment (Nyffeler et al., 2022; Harrill et al., 2021; Tsai et al., 2023; Johnson et al., 2022). Interestingly, a study by (Reardon et al., 2021) examined PFAS-associated *in vitro* tPODs in primary human liver spheroids and demonstrated that they may be more “protective” in comparison to apical PODs derived from animal studies for most chemicals analyzed, which further demonstrated the value of the use of *in vitro* transcriptomic data in risk assessment.

Accordingly, we aimed to analyze gene expression data in this study with respect to concentration-response. Several previous publications explored gene expression effects of PFAS (Houck et al., 2021; Reardon et al., 2021; Rowan-Carroll et al., 2021; Louisse et al., 2023; Marques et al., 2022; Behr et al., 2020), but few conducted formal transcriptomic benchmark dose analysis and derived points of departure. Two studies used primary human liver spheroids and assessed *in vitro* transcriptomic dose responses of PFAS treatment (Reardon et al., 2021; Rowan-Carroll et al., 2021). Specifically, Reardon et al (2021) found that PFAS-elicited transcriptomic effects (tPODs) ranged from 8.2 μM to 19.5 μM. Rowan-Carroll et al. (2021) reported that tPODs ranged from 8.2 μM to 53.5 μM. Compared with these two studies, tPODs derived herein were at the lower end (0.03 μM to 10 μM),

suggesting that iPSC-Hep could be a more sensitive *in vitro* model for screening-level risk assessments.

In addition to deriving the tPODs, we also sought to explore the relationship between a common tPOD derivation approach – the most sensitive pathway/gene set – that captures molecular pathway/gene set-level bioactivity and the number of CRGs effected by each compound in either cell type. The number of CRGs following chemical exposure has been used as a quantitative indicator of chemical's potency to enable comparative analysis across and within chemicals/groups (House et al., 2022; House et al., 2017). In addition, CRGs have been proposed to be useful for establishing quantitative thresholds to classify chemicals based on their potential to induce specific outcomes (Ramaiahgari et al., 2019). Our findings indicated that concordance between tPODs and numbers of CRGs was only observed in iPSC-Hep, but not in iPSC-CM. This finding suggests that associations between tPOD-based potency (derived from the most sensitive pathway/gene set) with the overall transcriptomic effect (as determined by the number of CRGs) is cell-type specific. The lack of correlation observed in iPSC-CM may be in part explained by the comparatively smaller evidence base on gene expression effects of chemicals in cardiomyocytes and thus, not as advanced of an understanding of the molecular pathways/gene sets that may be impacted (Hudson et al., 2012; Khatri et al., 2012). While *in vivo* and *in vitro* studies have demonstrated comparable tPOD values using different derivation approaches, these tPODs were often derived from few tissues (Farmahin et al., 2017; Thomas et al., 2013) or specific cell types (Reardon et al., 2023). The cell type-specificity observed in this study underscores the necessity for further research to determine what impact certain tPOD derivation approaches, and tissues or cells from which they originate, may have on the sensitivity of these "alternative" PODs especially as they are proposed for wider use in decision-making (U.S. EPA, 2023).

Prioritization and Risk Characterization of PFAS using pPODs and tPODs

The BER approach has been proposed as a high-throughput means of identifying potential risks and guiding the prioritization of substances for higher-tier evaluations (Wetmore et al., 2015; Sipes et al., 2017; Paul Friedman et al., 2020). Here we applied a highly conservative approach by using the minimum POD for each individual PFAS for the BER derivation, regardless of cell type and assay. We found that both iPSC-Hep and iPSC-CM contributed equally to the lowest PODs, and transcriptomic data contributed 14 of 18 lowest PODs. These findings underscore the value of both the cell models and also emphasize the importance of incorporating both the phenotypic and transcriptomic data for prioritization of PFAS using "protective" *in vitro* data.

We found that the BERs for most PFAS tested in this study ranged from 1 to 100. The overall range of BERs for PFAS in this study is consistent with previous *in vitro* PFAS studies that took a risk-based approach to interpretation of their *in vitro* data. For example, (Burnett et al., 2021b) demonstrated relatively narrow margins of exposure (<100) for most PFAS tested using iPSC-CM phenotypic assays. Rowan-Carroll et al. (2021) also reported a BER for PFOA within one order of magnitude of our study. It should be noted that 3 compounds (PFBS, 8:2 FTS and NH4PFOA) in our study had the BERs lower than 1. This apparent indication of a potential high risk was examined further. Both NH4PFOA

and PFBS had the highest exposure prediction values after IVIVE transformation (20.5 and 0.43 μM, respectively) among all 26 tested compounds; 8:2 FTS had a very low tPOD (0.04 μM). We need to acknowledge the limitations with the BER approach for PFAS. First, this study utilized two cell types that represent liver and heart to derive quantitative estimates of bioactivity. While hepatocytes and cardiomyocytes are the primary functional cells in these organs, they may not fully represent complex cell-cell interactions *in vivo*. Therefore, our bioactivity data may not adequately capture organ-level effects. Additional studies in more complex *in vitro* models, as well as cells that represent other tissues, are needed. Second, exposure values used in our study were based on *in silico* predictions rather than empirical data. Third, multiple data sources that we used to inform IVIVE have limitations with respect to the uncertainties in chemical-specific kinetic information for PFAS (Kreutz et al., 2023; Smeltz et al., 2023). Collectively, the uncertainty in BER estimates for PFAS is considerable and more confident toxicokinetic data is needed for these substances. In addition, despite our best efforts to maximize the number of PFAS for which BERs could be calculated, there were still 8 out of 26 PFAS with insufficient exposure prediction or Css data for the extrapolation. This underscores the importance of establishing PFAS-specific toxicokinetic and exposure data for large scale risk prioritization. Still, despite the limitations in the IVIVE process and subsequent BER calculation, the overall workflow herein effectively utilizes existing data and computational tools to enable an informative risk characterization approach that could also be applied for prioritizing PFAS.

Conclusion

This study pursued two main objectives, (i) to integrate transcriptomic and phenotypic data from two human *in vitro* cell models to gain insights into structure-effect relationships for PFAS, and (ii) to characterize potential risks of PFAS based on both bioactivity and predicted exposures. We observed that a number of PFAS had effects on iPSC-CM, supporting limited epidemiological data on the potential for these chemicals to have adverse effects on the heart rhythm. Even though a number of cell type- and substance-specific effects were observed, these effects did not align with the structure-based classification; we found that many of the tested PFAS elicited similar gene expression signatures. These results imply that existing classification proposals may not be suitable for “dimensionality reduction” among PFAS and show that additional research is needed to identify appropriate groupings for read-across. While our data revealed a relatively low risk for almost all tested compounds, even when using most conservative estimates for hazard and exposure, we also acknowledge considerable uncertainties in this approach because of the paucity of relevant toxicokinetic and exposure information. Overall, our results suggest that future considerations of hazards and risks of PFAS may require testing of the individual compounds, rather than representative members of various groups, and that additional studies are needed to inform grouping strategies and risk characterization.

Supplementary Material

Refer to Web version on PubMed Central for supplementary material.

Acknowledgements

The authors appreciate technical assistance with the experiments from Dr. Sarah D. Burnett (CTEH) and valuable discussions with Drs. Weihsueh A. Chiu (Texas A&M University) and George Daston (Procter & Gamble).

Funding

This work was supported, in part, by grants from the National Institute of Environmental Health Sciences (P42 ES027704 and T32 ES026568) and US Environmental Protection Agency (STAR RD83580201 and RD84045001). This publication contents are solely the responsibility of the grantee and do not necessarily represent the official views of the funding agencies. Further, funding agencies do not endorse the purchase of any commercial products or services mentioned in the publication.

Data availability

Gene expression data and experimental metadata are available in the Gene Expression Omnibus (https://www.ncbi.nlm.nih.gov/geo/query/acc.cgi?acc=GSE244110, reviewer token: ytangkkadbkvzgf). All supplementary data described in this manuscript are made public.

References

Amstutz VH, Cengo A, Gehres F. et al. (2022). Investigating the cytotoxicity of per- and polyfluoroalkyl substances in HepG2 cells: A structure-activity relationship approach. Toxicology 480, 153312. 10.1016/j.tox.2022.153312 [PubMed: 36075290]

Anderson JK, Brecher RW, Cousins IT et al. (2022). Grouping of PFAS for human health risk assessment: Findings from an independent panel of experts. Regul Toxicol Pharmacol 134, 105226. 10.1016/j.yrtph.2022.105226 [PubMed: 35817206]

Ball N, Cronin MT, Shen J. et al. (2016). Toward Good Read-Across Practice (GRAP) guidance. ALTEX 33, 149–166. 10.14573/altex.1601251 [PubMed: 26863606]

Behr AC, Plinsch C, Braeuning A. et al. (2020). Activation of human nuclear receptors by perfluoroalkylated substances (PFAS). Toxicol In Vitro 62, 104700. 10.1016/j.tiv.2019.104700 [PubMed: 31676336]

Bijland S, Rensen PC, Pieterman EJ et al. (2011). Perfluoroalkyl sulfonates cause alkyl chain length-dependent hepatic steatosis and hypolipidemia mainly by impairing lipoprotein production in APOE*3-Leiden CETP mice. Toxicol Sci 123, 290–303. 10.1093/toxsci/kfr142 [PubMed: 21705711]

Bjork JA, Butenhoff JL and Wallace KB (2011). Multiplicity of nuclear receptor activation by PFOA and PFOS in primary human and rodent hepatocytes. Toxicology 288, 8–17. 10.1016/j.tox.2011.06.012 [PubMed: 21723365]

Blanchette AD, Burnett SD, Grimm FA et al. (2020). A Bayesian Method for Population-wide Cardiotoxicity Hazard and Risk Characterization Using an In Vitro Human Model. Toxicol Sci 178, 391–403. 10.1093/toxsci/kfaa151 [PubMed: 33078833]

Buck RC, Franklin J, Berger U. et al. (2011). Perfluoroalkyl and polyfluoroalkyl substances in the environment: terminology, classification, and origins. Integr Environ Assess Manag 7, 513–541. 10.1002/ieam.258 [PubMed: 21793199]

Buck RC, Korzeniowski SH, Laganis E. et al. (2021). Identification and classification of commercially relevant per- and poly-fluoroalkyl substances (PFAS). Integr Environ Assess Manag 17, 1045–1055. 10.1002/ieam.4450 [PubMed: 33991049]

Burnett SD, Blanchette AD, Grimm FA et al. (2019). Population-based toxicity screening in human induced pluripotent stem cell-derived cardiomyocytes. Toxicol Appl Pharmacol 381, 114711. 10.1016/j.taap.2019.114711 [PubMed: 31425687]

Burnett SD, Blanchette AD, Chiu WA et al. (2021a). Human induced pluripotent stem cell (iPSC)-derived cardiomyocytes as an in vitro model in toxicology: strengths and weaknesses for

hazard identification and risk characterization. Expert Opin Drug Metab Toxicol 17, 887–902. 10.1080/17425255.2021.1894122 [PubMed: 33612039]

Burnett SD, Blanchette AD, Chiu WA et al. (2021b). Cardiotoxicity Hazard and Risk Characterization of ToxCast Chemicals Using Human Induced Pluripotent Stem Cell-Derived Cardiomyocytes from Multiple Donors. Chem Res Toxicol 34, 2110–2124. 10.1021/acs.chemrestox.1c00203 [PubMed: 34448577]

Carlson LM, Angrish M, Shirke AV et al. (2022). Systematic Evidence Map for Over One Hundred and Fifty Per- and Polyfluoroalkyl Substances (PFAS). Environ Health Perspect 130, 56001. 10.1289/EHP10343 [PubMed: 35580034]

Carstens KE, Freudenrich T, Wallace K. et al. (2023). Evaluation of Per- and Polyfluoroalkyl Substances (PFAS) In Vitro Toxicity Testing for Developmental Neurotoxicity. Chem Res Toxicol 36, 402–419. 10.1021/acs.chemrestox.2c00344 [PubMed: 36821828]

Chen Z, Jang S, Kaihatu JM et al. (2021). Potential Human Health Hazard of Post-Hurricane Harvey Sediments in Galveston Bay and Houston Ship Channel: A Case Study of Using In Vitro Bioactivity Data to Inform Risk Management Decisions. Int J Environ Res Public Health 18, 13378. 10.3390/ijerph182413378 [PubMed: 34948986]

Cheng W, Yu Z, Feng L. et al. (2013). Perfluorooctane sulfonate (PFOS) induced embryotoxicity and disruption of cardiogenesis. Toxicol In Vitro 27, 1503–1512. 10.1016/j.tiv.2013.03.014 [PubMed: 23562911]

Cheng W. and Ng CA (2018). Predicting Relative Protein Affinity of Novel Per- and Polyfluoroalkyl Substances (PFASs) by An Efficient Molecular Dynamics Approach. Environ Sci Technol 52, 7972–7980. 10.1021/acs.est.8b01268 [PubMed: 29897239]

Cheng W, Li M, Zhang L. et al. (2023). Close association of PFASs exposure with hepatic fibrosis than steatosis: evidences from NHANES 2017–2018. Ann Med 55, 2216943. 10.1080/07853890.2023.2216943 [PubMed: 37323015]

Cousins IT, DeWitt JC, Gluge J. et al. (2020). Strategies for grouping per- and polyfluoroalkyl substances (PFAS) to protect human and environmental health. Environ Sci Process Impacts 22, 1444–1460. 10.1039/d0em00147c [PubMed: 32495786]

Curran I, Hierlihy SL, Liston V. et al. (2008). Altered fatty acid homeostasis and related toxicologic sequelae in rats exposed to dietary potassium perfluorooctanesulfonate (PFOS). J Toxicol Environ Health A 71, 1526–1541. 10.1080/15287390802361763 [PubMed: 18923995]

Das KP, Wood CR, Lin MT et al. (2017). Perfluoroalkyl acids-induced liver steatosis: Effects on genes controlling lipid homeostasis. Toxicology 378, 37–52. 10.1016/j.tox.2016.12.007 [PubMed: 28049043]

David N, Antignac JP, Roux M. et al. (2023). Associations between perfluoroalkyl substances and the severity of non-alcoholic fatty liver disease. Environ Int 180, 108235. 10.1016/j.envint.2023.108235 [PubMed: 37776622]

Davidsen N, Rosenmai AK, Lauschke K. et al. (2021). Developmental effects of PFOS, PFOA and GenX in a 3D human induced pluripotent stem cell differentiation model. Chemosphere 279, 130624. 10.1016/j.chemosphere.2021.130624 [PubMed: 34134420]

Davidsen N, Ramhoj L, Kugathas I. et al. (2022). PFOS disrupts key developmental pathways during hiPSC-derived cardiomyocyte differentiation in vitro. Toxicol In Vitro 85, 105475. 10.1016/j.tiv.2022.105475 [PubMed: 36116746]

Dawson DE, Lau C, Pradeep P. et al. (2023). A Machine Learning Model to Estimate Toxicokinetic Half-Lives of Per- and Polyfluoro-Alkyl Substances (PFAS) in Multiple Species. Toxics 11, 10.3390/toxics11020098

Dobin A, Davis CA, Schlesinger F. et al. (2013). STAR: ultrafast universal RNA-seq aligner. Bioinformatics 29, 15–21. 10.1093/bioinformatics/bts635 [PubMed: 23104886]

ECHA (2023). Per- and polyfluoroalkyl substances (PFAS). https://echa.europa.eu/hot-topics/perfluoroalkyl-chemicals-pfas, Acessed on: July 11

Fang H, Knezevic B, Burnham KL et al. (2016). XGR software for enhanced interpretation of genomic summary data, illustrated by application to immunological traits. Genome Med 8, 129. 10.1186/s13073-016-0384-y [PubMed: 27964755]

Farmahin R, Williams A, Kuo B. et al. (2017). Recommended approaches in the application of toxicogenomics to derive points of departure for chemical risk assessment. Arch Toxicol 91, 2045–2065. 10.1007/s00204-016-1886-5 [PubMed: 27928627]

Farr S. and Dunn RT (1999). Concise review: gene expression applied to toxicology. Toxicol.Sci 50, 1–9. [PubMed: 10445747]

Fenton SE, Ducatman A, Boobis A. et al. (2021). Per- and Polyfluoroalkyl Substance Toxicity and Human Health Review: Current State of Knowledge and Strategies for Informing Future Research. Environ Toxicol Chem 40, 606–630. 10.1002/etc.4890 [PubMed: 33017053]

Gomis MI, Vestergren R, Borg D. et al. (2018). Comparing the toxic potency in vivo of long-chain perfluoroalkyl acids and fluorinated alternatives. Environ Int 113, 1–9. 10.1016/j.envint.2018.01.011 [PubMed: 29421396]

Grimm FA, Iwata Y, Sirenko O. et al. (2015). High-Content Assay Multiplexing for Toxicity Screening in Induced Pluripotent Stem Cell-Derived Cardiomyocytes and Hepatocytes. Assay Drug Dev Technol 13, 529–546. 10.1089/adt.2015.659 [PubMed: 26539751]

Grimm FA, Iwata Y, Sirenko O. et al. (2016). A chemical-biological similarity-based grouping of complex substances as a prototype approach for evaluating chemical alternatives. Green Chem 18, 4407–4419. 10.1039/c6gc01147k [PubMed: 28035192]

Grimm FA, Blanchette A, House JS et al. (2018). A human population-based organotypic in vitro model for cardiotoxicity screening. ALTEX 35, 441–452. 10.14573/altex.1805301 [PubMed: 29999168]

Harrill JA, Everett LJ, Haggard DE et al. (2021). High-Throughput Transcriptomics Platform for Screening Environmental Chemicals. Toxicol Sci 181, 68–89. 10.1093/toxsci/kfab009 [PubMed: 33538836]

Hickey NJ, Crump D, Jones SP et al. (2009). Effects of 18 perfluoroalkyl compounds on mRNA expression in chicken embryo hepatocyte cultures. Toxicol Sci 111, 311–320. 10.1093/toxsci/kfp160 [PubMed: 19617454]

Ho SH, Soh SXH, Wang MX et al. (2022). Perfluoroalkyl substances and lipid concentrations in the blood: A systematic review of epidemiological studies. Sci Total Environ 850, 158036. 10.1016/j.scitotenv.2022.158036 [PubMed: 35973530]

Houck KA, Patlewicz G, Richard AM et al. (2021). Bioactivity profiling of per- and polyfluoroalkyl substances (PFAS) identifies potential toxicity pathways related to molecular structure. Toxicology 457, 152789. 10.1016/j.tox.2021.152789 [PubMed: 33887376]

Houck KA, Friedman KP, Feshuk M. et al. (2023). Evaluation of 147 perfluoroalkyl substances for immunotoxic and other (patho)physiological activities through phenotypic screening of human primary cells. ALTEX 40, 248–270. 10.14573/altex.2203041 [PubMed: 36129398]

House JS, Grimm FA, Jima DD et al. (2017). A Pipeline for High-Throughput Concentration Response Modeling of Gene Expression for Toxicogenomics. Front Genet 8, 168. 10.3389/fgene.2017.00168 [PubMed: 29163636]

House JS, Grimm FA, Klaren WD et al. (2021). Grouping of UVCB substances with new approach methodologies (NAMs) data. ALTEX 38, 123–137. 10.14573/altex.2006262 [PubMed: 33086383]

House JS, Grimm FA, Klaren WD et al. (2022). Grouping of UVCB substances with dose-response transcriptomics data from human cell-based assays. ALTEX 39, 388–404. 10.14573/altex.2107051 [PubMed: 35288757]

Hudson NJ, Dalrymple BP and Reverter A. (2012). Beyond differential expression: the quest for causal mutations and effector molecules. BMC Genomics 13, 356. 10.1186/1471-2164-13-356 [PubMed: 22849396]

Jassal B, Matthews L, Viteri G. et al. (2020). The reactome pathway knowledgebase. Nucleic Acids Res 48, D498–D503. 10.1093/nar/gkz1031 [PubMed: 31691815]

Johnson KJ, Auerbach SS and Costa E. (2020). A Rat Liver Transcriptomic Point of Departure Predicts a Prospective Liver or Non-liver Apical Point of Departure. Toxicol Sci 176, 86–102. 10.1093/toxsci/kfaa062 [PubMed: 32384157]

Johnson KJ, Auerbach SS, Stevens T. et al. (2022). A Transformative Vision for an Omics-Based Regulatory Chemical Testing Paradigm. Toxicol Sci 190, 127–132. 10.1093/toxsci/kfac097 [PubMed: 36165699]

Khatri P, Sirota M. and Butte AJ (2012). Ten years of pathway analysis: current approaches and outstanding challenges. PLoS Comput Biol 8, e1002375. 10.1371/journal.pcbi.1002375

Kreutz A, Clifton MS, Henderson WM et al. (2023). Category-Based Toxicokinetic Evaluations of Data-Poor Per- and Polyfluoroalkyl Substances (PFAS) using Gas Chromatography Coupled with Mass Spectrometry. Toxics 11, 463. 10.3390/toxics11050463 [PubMed: 37235277]

LaRocca J, Johnson KJ, LeBaron MJ et al. (2017). The interface of epigenetics and toxicology in product safety assessment. Current Opinion in Toxicology 6, 87–92. 10.1016/j.cotox.2017.11.004

Lind L, Araujo JA, Barchowsky A. et al. (2021). Consensus on the Key Characteristics of Cardiovascular Toxicants. (submitted)

Louisse J, Fragki S, Rijkers D. et al. (2023). Determination of in vitro hepatotoxic potencies of a series of perfluoroalkyl substances (PFASs) based on gene expression changes in HepaRG liver cells. Arch Toxicol 97, 1113–1131. 10.1007/s00204-023-03450-2 [PubMed: 36864359]

Love MI, Huber W. and Anders S. (2014). Moderated estimation of fold change and dispersion for RNA-seq data with DESeq2. Genome Biol 15, 550. 10.1186/s13059-014-0550-8 [PubMed: 25516281]

Marques E, Pfohl M, Wei W. et al. (2022). Replacement per- and polyfluoroalkyl substances (PFAS) are potent modulators of lipogenic and drug metabolizing gene expression signatures in primary human hepatocytes. Toxicol Appl Pharmacol 442, 115991. 10.1016/j.taap.2022.115991 [PubMed: 35337807]

Massachusetts Government (2020). Massachusetts PFAS Drinking Water Standard (MCL). https://www.mass.gov/lists/massachusetts-pfas-drinking-water-standard-mcl, Acessed on: July 4th 2023.

Meneguzzi A, Fava C, Castelli M. et al. (2021). Exposure to Perfluoroalkyl Chemicals and Cardiovascular Disease: Experimental and Epidemiological Evidence. Front Endocrinol (Lausanne) 12, 706352. 10.3389/fendo.2021.706352 [PubMed: 34305819]

Menger F, Pohl J, Ahrens L. et al. (2020). Behavioural effects and bioconcentration of per- and polyfluoroalkyl substances (PFASs) in zebrafish (Danio rerio) embryos. Chemosphere 245, 125573. 10.1016/j.chemosphere.2019.125573 [PubMed: 31877453]

Naile JE, Wiseman S, Bachtold K. et al. (2012). Transcriptional effects of perfluorinated compounds in rat hepatoma cells. Chemosphere 86, 270–277. 10.1016/j.chemosphere.2011.09.044 [PubMed: 22071372]

National Academies of Sciences Engineering and Medicine (2022). Guidance on PFAS Exposure, Testing, and Clinical Follow-Up. Washington, DC: The National Academies Press. https://nap.nationalacademies.org/catalog/26156/guidance-on-pfas-exposure-testing-and-clinical-follow-up doi:10.17226/26156

National Toxicology Program (2018). NTP Research Report on National Toxicology Program Approach to Genomic Dose-Response Modeling: Research Report 5. https://www.ncbi.nlm.nih.gov/pubmed/30321009 10.22427/NTP-RR-5, Acessed on:

National Toxicology Program (2019a). Toxicity studies of perfluoroalkyl sulfonates administered by gavage to Sprague Dawley (Hsd:Sprague Dawley SD) rats (revised). Toxic Rep Ser 10.22427/NTP-TOX-96

National Toxicology Program (2019b). Toxicity studies of perfluoroalkyl carboxylates administered by gavage to Sprague Dawley (Hsd:Sprague Dawley SD) rats (revised). Toxic Rep Ser 10.22427/NTP-TOX-97

Nyffeler J, Willis C, Harris FR et al. (2022). Combining phenotypic profiling and targeted RNA-Seq reveals linkages between transcriptional perturbations and chemical effects on cell morphology: Retinoic acid as an example. Toxicol Appl Pharmacol 444, 116032. 10.1016/j.taap.2022.116032 [PubMed: 35483669]

Environment Directorate, ORGANISATION FOR ECONOMIC COOPERATION AND DEVELOPMENT (2018). Toward a New Comprehensive Global Database of Per-and Polyfluoroalkyl Substances (PFASs): Summary Report on Updating the OECD 2007 List of Per and Polyfluoroalkyl Substances (PFASs). Acessed on: July 4th 2023.th

Patlewicz G, Richard AM, Williams AJ et al. (2019). A Chemical Category-Based Prioritization Approach for Selecting 75 Per- and Polyfluoroalkyl Substances (PFAS) for Tiered Toxicity

and Toxicokinetic Testing. Environ Health Perspect 127, 14501. 10.1289/EHP4555 [PubMed: 30632786]

Patlewicz G, Richard AM, Williams AJ et al. (2022). Towards reproducible structure-based chemical categories for PFAS to inform and evaluate toxicity and toxicokinetic testing. Comput Toxicol 24, 100250. 10.1016/j.comtox.2022.100250

Paul Friedman K, Gagne M, Loo LH et al. (2020). Utility of In Vitro Bioactivity as a Lower Bound Estimate of In Vivo Adverse Effect Levels and in Risk-Based Prioritization. Toxicol Sci 173, 202–225. 10.1093/toxsci/kfz201 [PubMed: 31532525]

Pearce RG, Setzer RW, Strope CL et al. (2017). httk: R Package for High-Throughput Toxicokinetics. J Stat Softw 79, 1–26. 10.18637/jss.v079.i04 [PubMed: 30220889]

Phillips JR, Svoboda DL, Tandon A. et al. (2019). BMDExpress 2: enhanced transcriptomic dose-response analysis workflow. Bioinformatics 35, 1780–1782. 10.1093/bioinformatics/bty878 [PubMed: 30329029]

Qi Q, Niture S, Gadi S. et al. (2023). Per- and polyfluoroalkyl substances activate UPR pathway, induce steatosis and fibrosis in liver cells. Environ Toxicol 38, 225–242. 10.1002/tox.23680 [PubMed: 36251517]

Ramaiahgari SC, Auerbach SS, Saddler TO et al. (2019). The Power of Resolution: Contextualized Understanding of Biological Responses to Liver Injury Chemicals Using High-throughput Transcriptomics and Benchmark Concentration Modeling. Toxicol Sci 169, 553–566. 10.1093/toxsci/kfz065 [PubMed: 30850835]

Reardon AJF, Rowan-Carroll A, Ferguson SS et al. (2021). Potency Ranking of Per- and Polyfluoroalkyl Substances Using High-Throughput Transcriptomic Analysis of Human Liver Spheroids. Toxicol Sci 184, 154–169. 10.1093/toxsci/kfab102 [PubMed: 34453843]

Reardon AJF, Farmahin R, Williams A. et al. (2023). From vision toward best practices: Evaluating in vitro transcriptomic points of departure for application in risk assessment using a uniform workflow. Front Toxicol 5, 1194895. 10.3389/ftox.2023.1194895 [PubMed: 37288009]

Ring CL, Arnot JA, Bennett DH et al. (2019). Consensus Modeling of Median Chemical Intake for the U.S. Population Based on Predictions of Exposure Pathways. Environ Sci Technol 53, 719–732. 10.1021/acs.est.8b04056 [PubMed: 30516957]

Robarts DR, Venneman KK, Gunewardena S. et al. (2022). GenX induces fibroinflammatory gene expression in primary human hepatocytes. Toxicology 477, 153259. 10.1016/j.tox.2022.153259 [PubMed: 35850385]

Rowan-Carroll A, Reardon A, Leingartner K. et al. (2021). High-Throughput Transcriptomic Analysis of Human Primary Hepatocyte Spheroids Exposed to Per- and Polyfluoroalkyl Substances as a Platform for Relative Potency Characterization. Toxicol Sci 181, 199–214. 10.1093/toxsci/kfab039 [PubMed: 33772556]

Rusyn I, Arzuaga X, Cattley RC et al. (2021). Key Characteristics of Human Hepatotoxicants as a Basis for Identification and Characterization of the Causes of Liver Toxicity. Hepatology 74, 3486–3496. 10.1002/hep.31999 [PubMed: 34105804]

Schillemans T, Donat-Vargas C. and Akesson A. (2023). Per- and polyfluoroalkyl substances and cardiometabolic diseases: a review. Basic Clin Pharmacol Toxicol 10.1111/bcpt.13949

Sha B, Schymanski EL, Ruttkies C. et al. (2019). Exploring open cheminformatics approaches for categorizing per- and polyfluoroalkyl substances (PFASs). Environ Sci Process Impacts 21, 1835–1851. 10.1039/c9em00321e [PubMed: 31576380]

Sipes NS, Wambaugh JF, Pearce R. et al. (2017). An Intuitive Approach for Predicting Potential Human Health Risk with the Tox21 10k Library. Environ Sci Technol 51, 10786–10796. 10.1021/acs.est.7b00650 [PubMed: 28809115]

Sirenko O, Cromwell EF, Crittenden C. et al. (2013). Assessment of beating parameters in human induced pluripotent stem cells enables quantitative in vitro screening for cardiotoxicity. Toxicol Appl Pharmacol 273, 500–507. 10.1016/j.taap.2013.09.017 [PubMed: 24095675]

Sirenko O, Hesley J, Rusyn I. et al. (2014). High-content assays for hepatotoxicity using induced pluripotent stem cell-derived cells. Assay Drug Dev Technol 12, 43–54. 10.1089/adt.2013.520 [PubMed: 24229356]

Sirenko O, Grimm FA, Ryan KR et al. (2017). In vitro cardiotoxicity assessment of environmental chemicals using an organotypic human induced pluripotent stem cell-derived model. Toxicol Appl Pharmacol 322, 60–74. 10.1016/j.taap.2017.02.020 [PubMed: 28259702]

Smeltz M, Wambaugh JF and Wetmore BA (2023). Plasma Protein Binding Evaluations of Per- and Polyfluoroalkyl Substances for Category-Based Toxicokinetic Assessment. Chem Res Toxicol 36, 870–881. 10.1021/acs.chemrestox.3c00003 [PubMed: 37184865]

Solan ME and Lavado R. (2023). Effects of short-chain per- and polyfluoroalkyl substances (PFAS) on human cytochrome P450 (CYP450) enzymes and human hepatocytes: An in vitro study. Curr Res Toxicol 5, 100116. 10.1016/j.crtox.2023.100116 [PubMed: 37575337]

Soldatow VY, Lecluyse EL, Griffith LG et al. (2013). In vitro models for liver toxicity testing. Toxicol Res (Camb) 2, 23–39. 10.1039/C2TX20051A [PubMed: 23495363]

Subramanian A, Tamayo P, Mootha VK et al. (2005). Gene set enrichment analysis: a knowledge-based approach for interpreting genome-wide expression profiles. Proc Natl Acad Sci U S A 102, 15545–15550. 10.1073/pnas.0506580102 [PubMed: 16199517]

Tang LL, Wang JD, Xu TT et al. (2017). Mitochondrial toxicity of perfluorooctane sulfonate in mouse embryonic stem cell-derived cardiomyocytes. Toxicology 382, 108–116. 10.1016/j.tox.2017.03.011 [PubMed: 28288859]

Thomas RS, Clewell HJ 3rd, Allen BC et al. (2011). Application of transcriptional benchmark dose values in quantitative cancer and noncancer risk assessment. Toxicol Sci 120, 194–205. 10.1093/toxsci/kfq355 [PubMed: 21097997]

Thomas RS, Wesselkamper SC, Wang NC et al. (2013). Temporal concordance between apical and transcriptional points of departure for chemical risk assessment. Toxicol Sci 134, 180–194. 10.1093/toxsci/kft094 [PubMed: 23596260]

Tibshirani RJ and Efron B. (2002). Pre-validation and inference in microarrays. Stat Appl Genet Mol Biol 1, Article1.

Tsai HD, House JS, Wright FA et al. (2023). A tiered testing strategy based on in vitro phenotypic and transcriptomic data for selecting representative petroleum UVCBs for toxicity evaluation in vivo. Toxicol Sci 193, 219–233. 10.1093/toxsci/kfad041 [PubMed: 37079747]

US Environmental Protection Agency (2021). National PFAS Testing Strategy: Identification of Candidate Per- and Polyfluoroalkyl Substances (PFAS) for Testing. https://www.epa.gov/system/files/documents/2021-10/pfas-natl-test-strategy.pdf Acessed on: July 4th 2023.

US Environmental Protection Agency (2023). Standard Methods for Development of EPA Transcriptomic Assessment Products (ETAPs): External Review Draft. https://www.epa.gov/system/files/documents/2023-06/ETAP%20Standard%20Methods%20Doc_BOSC%20Report_Draft%20Final_5_19_23_508%20Tagged.pdf Acessed on: July 4th 2023.

US EPA (2019). Per, and Polyfluoroalkyl Substances (PFAS) Action Plan. Acessed on: July 4th 2023.

Vinken M, Knapen D, Vergauwen L. et al. (2017). Adverse outcome pathways: a concise introduction for toxicologists. Arch Toxicol 91, 3697–3707. 10.1007/s00204-017-2020-z [PubMed: 28660287]

Wambaugh JF, Setzer RW, Reif DM et al. (2013). High-throughput models for exposure-based chemical prioritization in the ExpoCast project. Environ Sci Technol 47, 8479–8488. 10.1021/es400482g [PubMed: 23758710]

Wan HT, Zhao YG, Wei X. et al. (2012). PFOS-induced hepatic steatosis, the mechanistic actions on beta-oxidation and lipid transport. Biochim Biophys Acta 1820, 1092–1101. 10.1016/j.bbagen.2012.03.010 [PubMed: 22484034]

Wang B, Zhang R, Jin F. et al. (2017). Perfluoroalkyl substances and endometriosis-related infertility in Chinese women. Environ Int 102, 207–212. 10.1016/j.envint.2017.03.003 [PubMed: 28283302]

Wetmore BA, Wambaugh JF, Ferguson SS et al. (2012). Integration of dosimetry, exposure, and high-throughput screening data in chemical toxicity assessment. Toxicol Sci 125, 157–174. 10.1093/toxsci/kfr254 [PubMed: 21948869]

Wetmore BA, Wambaugh JF, Allen B. et al. (2015). Incorporating High-Throughput Exposure Predictions With Dosimetry-Adjusted In Vitro Bioactivity to Inform Chemical Toxicity Testing. Toxicol Sci 148, 121–136. 10.1093/toxsci/kfv171 [PubMed: 26251325]

Wignall JA, Shapiro AJ, Wright FA et al. (2014). Standardizing benchmark dose calculations to improve science-based decisions in human health assessments. Environ Health Perspect 122, 499–505. 10.1289/ehp.1307539 [PubMed: 24569956]

Williams AJ, Grulke CM, Edwards J. et al. (2017). The CompTox Chemistry Dashboard: a community data resource for environmental chemistry. J Cheminform 9, 61. 10.1186/s13321-017-0247-6 [PubMed: 29185060]

Woodruff TJ, Rayasam SDG, Axelrad DA et al. (2023). A science-based agenda for health-protective chemical assessments and decisions: overview and consensus statement. Environ Health 21, 132. 10.1186/s12940-022-00930-3 [PubMed: 36635734]

Yu G. and He QY (2016). ReactomePA: an R/Bioconductor package for reactome pathway analysis and visualization. Mol Biosyst 12, 477–479. 10.1039/c5mb00663e [PubMed: 26661513]

Zhang L, Ren XM, Wan B. et al. (2014). Structure-dependent binding and activation of perfluorinated compounds on human peroxisome proliferator-activated receptor gamma. Toxicol Appl Pharmacol 279, 275–283. 10.1016/j.taap.2014.06.020 [PubMed: 24998974]

Zhang YY, Tang LL, Zheng B. et al. (2016). Protein profiles of cardiomyocyte differentiation in murine embryonic stem cells exposed to perfluorooctane sulfonate. J Appl Toxicol 36, 726–740. 10.1002/jat.3207 [PubMed: 26178269]

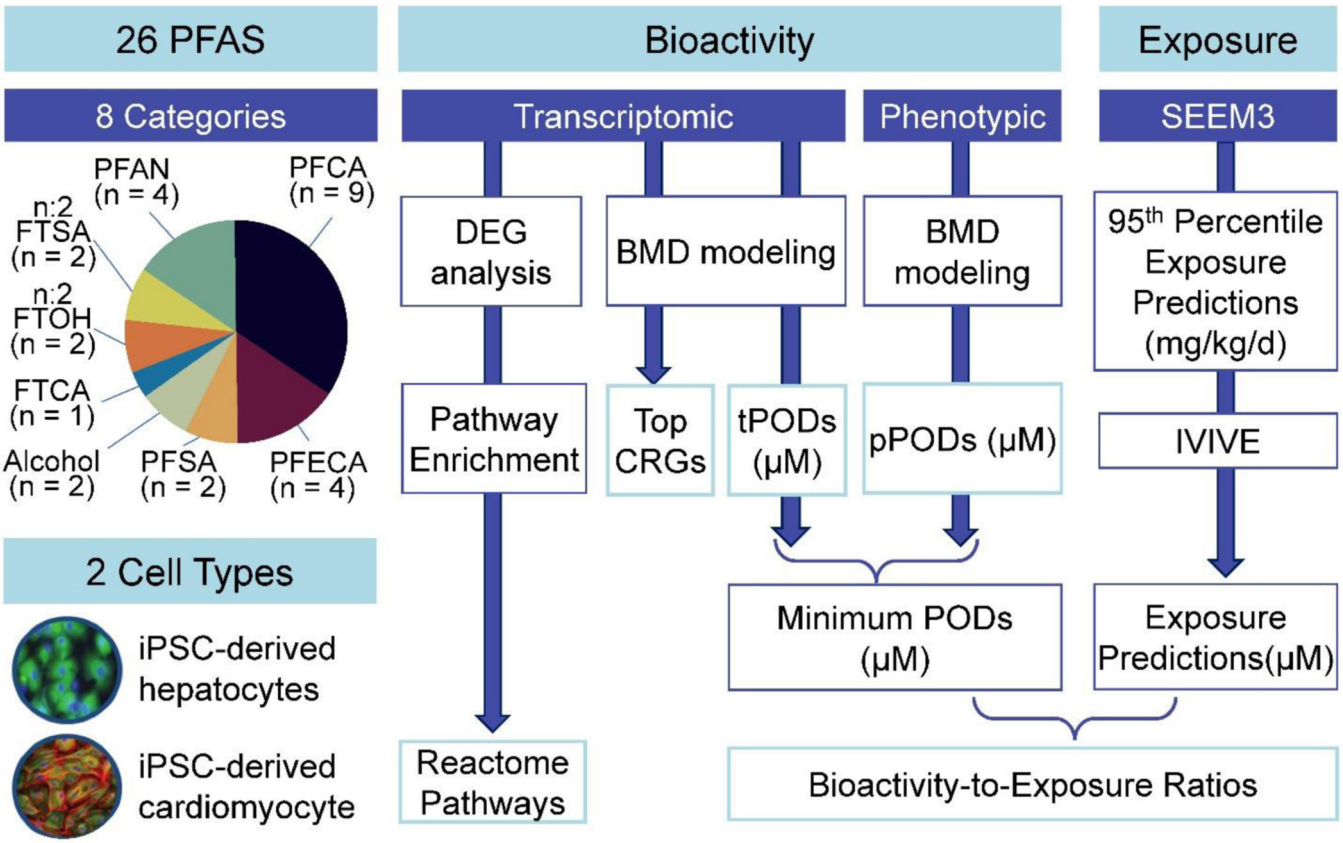

Fig. 1:

Overview of the study design and data analyses of the *in vitro* effects of 26 PFAS of iPSC-Hep and iPSC-CM. See abbreviations for PFAS classes in Tab. 1. Other abbreviations: DEG, differentially expressed genes; BMD, benchmark dose; CRG, concentration-response genes; POD, point of departure (t for transcriptomic and p for phenotypic data); IVIVE, in vitro-to-in vivo extrapolation.

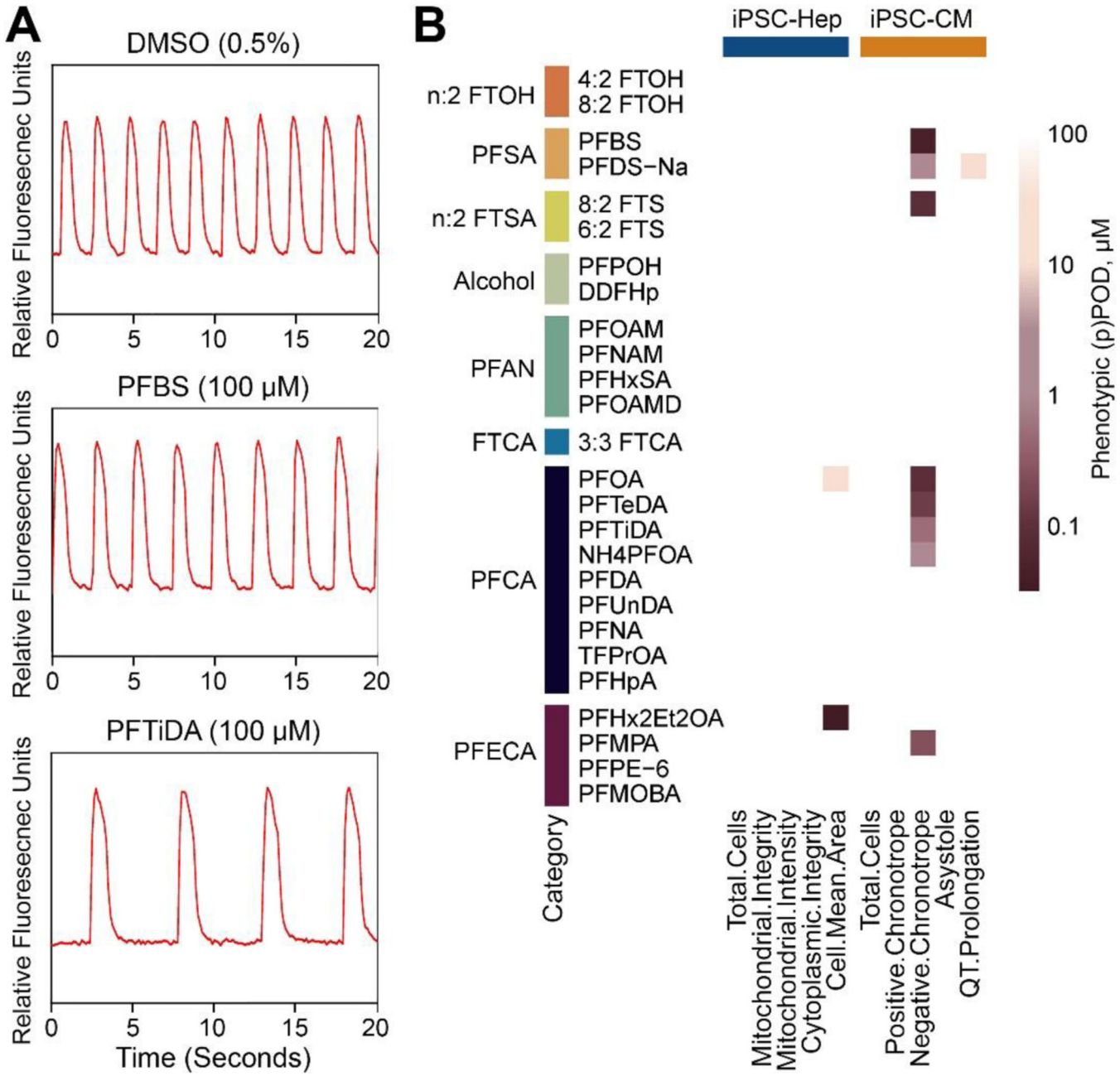

Fig. 2:

Phenotypic effects of PFAS on iPSC-Hep and iPSC-CM. **(A)** Representative Ca^{2+} flux traces (90 minutes after treatment) for vehicle (0.5% DMSO), PFBS (100 µM), or PFTiDA (100 µM) in iPSC-CM. **(B)** A heatmap illustrating phenotypic points of departure (pPOD) for the phenotypes (columns) evaluated in iPSC-Hep (on the left) and iPSC-CM (on the right) for each tested PFAS (rows). A darker color indicates a lower POD value. PFAS were grouped by chemical structure categories. See Tab. 1 for class and individual chemical abbreviations.

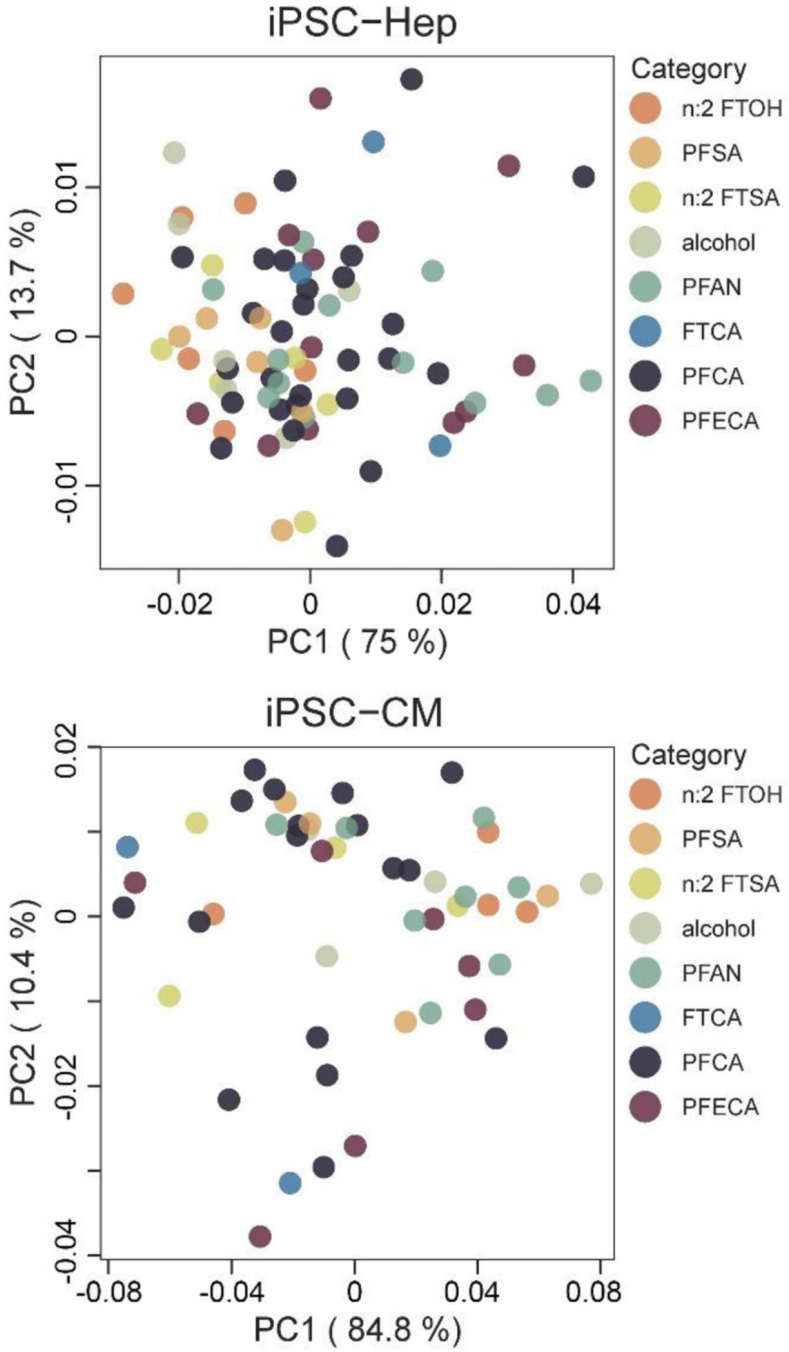

Fig. 3:

Principal Component (PC) Analysis of normalized gene expression data from iPSC-Hep (top) and iPSC-CM (bottom) treated with PFAS (10 μM). In both panels, a dot represents an individual sample, while the colors correspond to different PFAS categories as indicated in the legends. See Tab. 1. for class abbreviations.

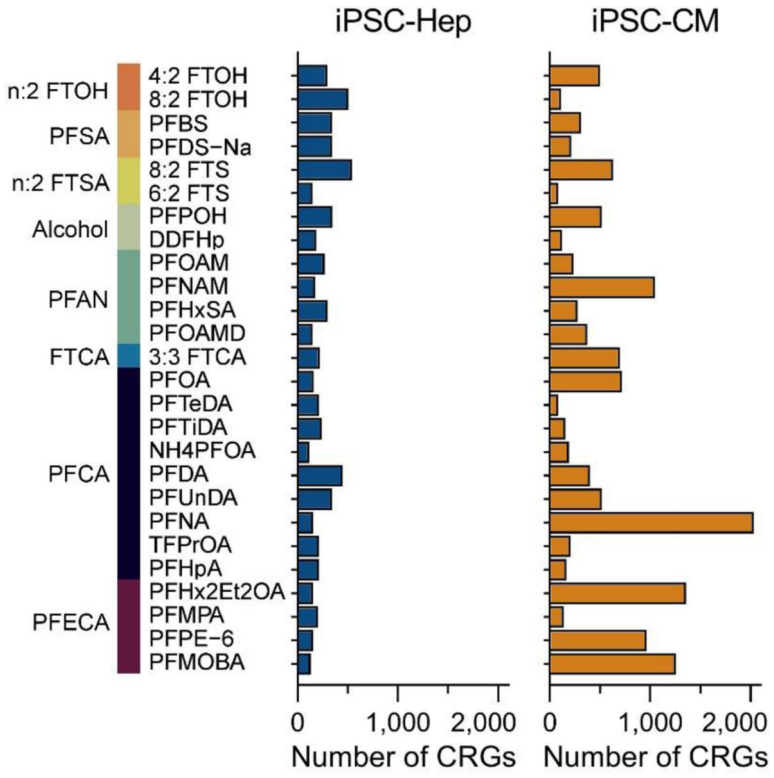

Fig. 4:

Bar plots illustrating the number of concentration responsive genes (CRGs) in iPSC-Hep (displayed as blue bars on the left) and iPSC-CM (shown as orange bars on the right) for each tested PFAS. The PFAS are ordered based on their respective categories. See Tab. 1 for class and individual chemical abbreviations.

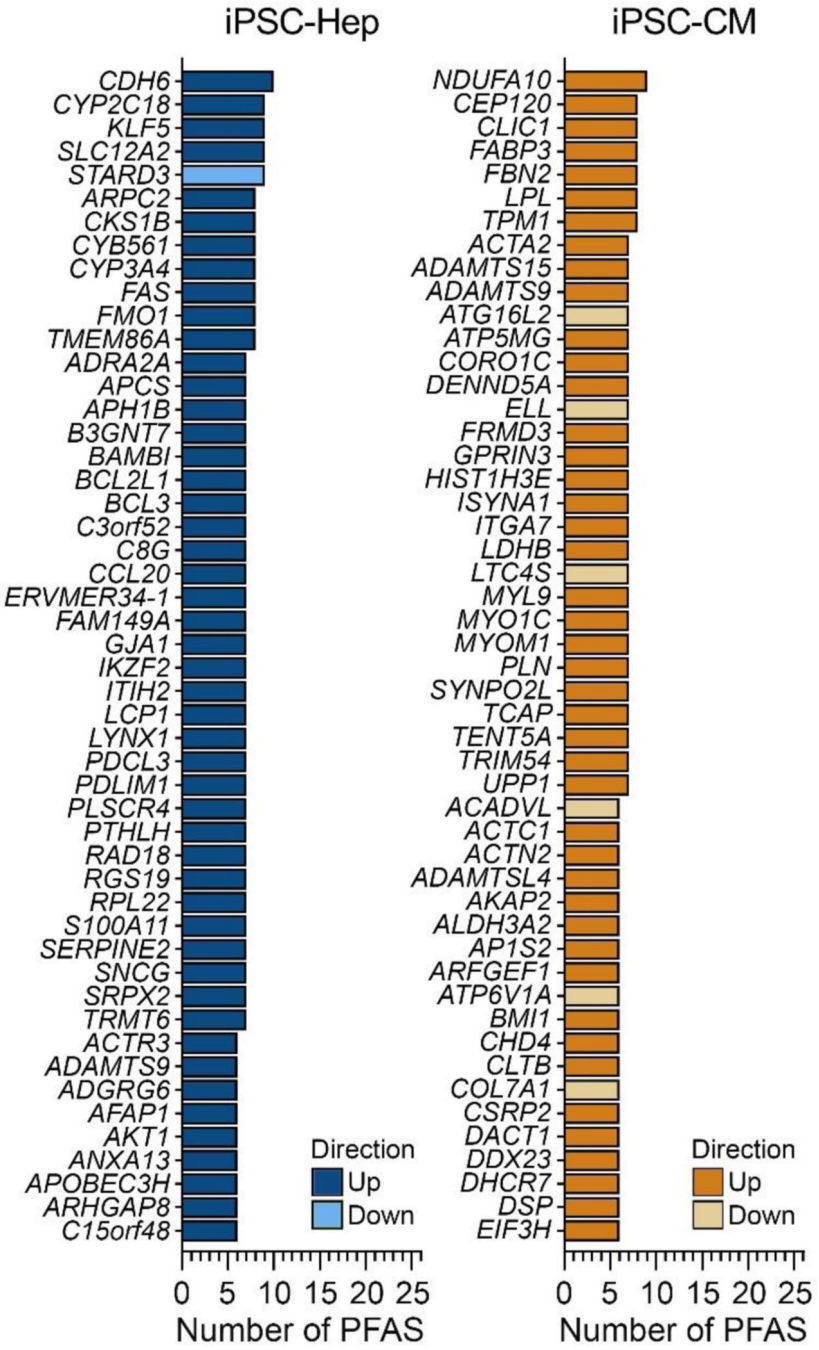

Fig. 5:

Bar plots displaying the top 50 common genes that exhibited concentration-responsive effects, ranked by the number of tested PFAS with significant impact (empirical p-value < 0.05, calculated using permutation) in iPSC-Hep (depicted as blue bars on the left) and iPSC-CM (illustrated as orange bars on the right. Bars with darker shades represent up-regulation and lighter shades represent down-regulation.

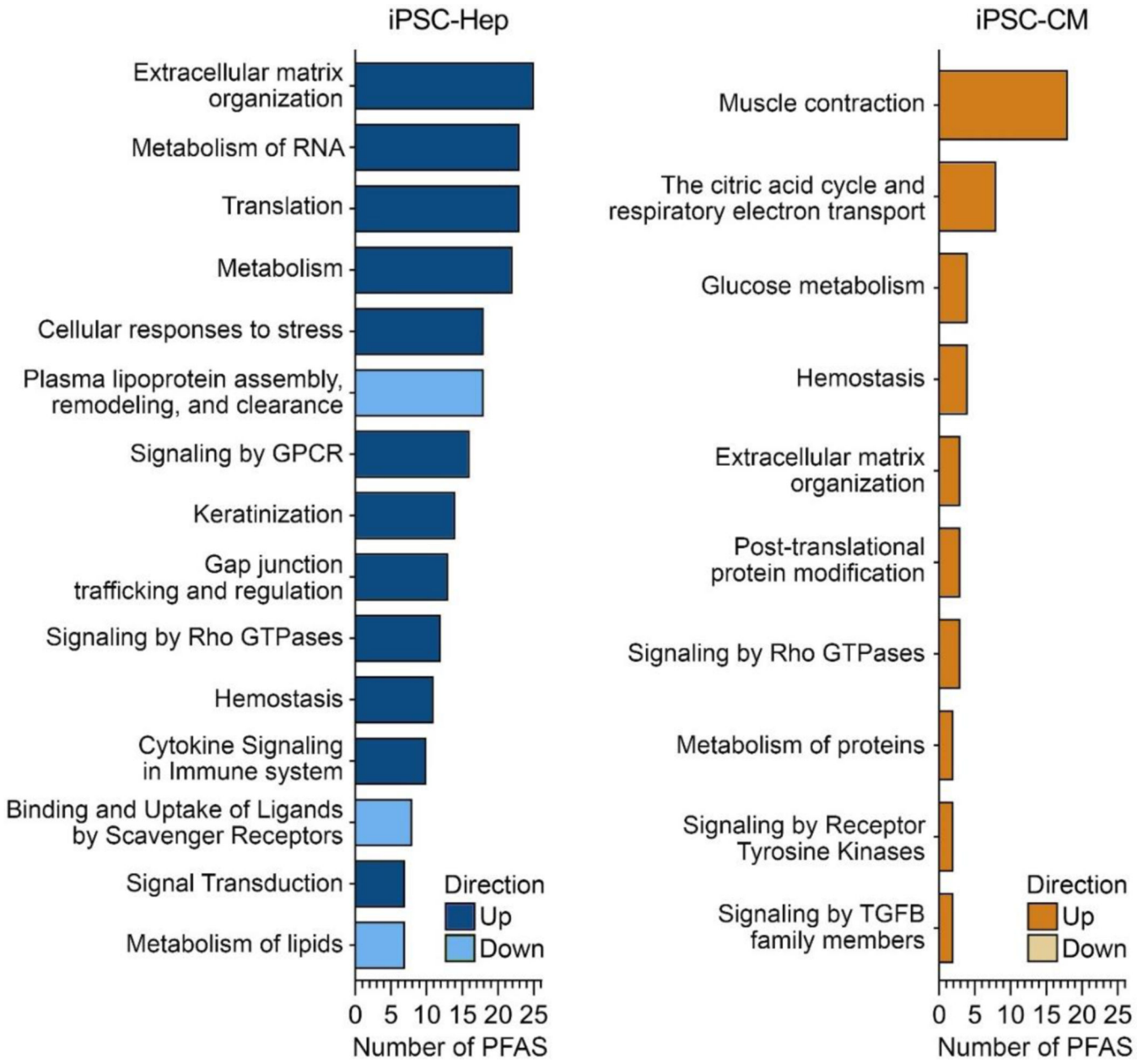

Fig. 6:

Bar plots presenting the top groups of Reactome pathways enriched in iPSC-Hep (depicted as blue bars on the left) and iPSC-CM (shown as orange bars on the right), ranked by the number of tested PFAS with significant effects (false discovery $q < 0.1$). Pathways are color-coded, with darker shades indicating up-regulated pathways and lighter shades representing down-regulated pathways. The pathways showcased in this figure are summarized based on shared higher-level categories, capturing overarching hierarchical relationships within Reactome pathways. See Supplementary Files 6 and 7 for the full list of enriched pathways and their corresponding upper-level groupings.

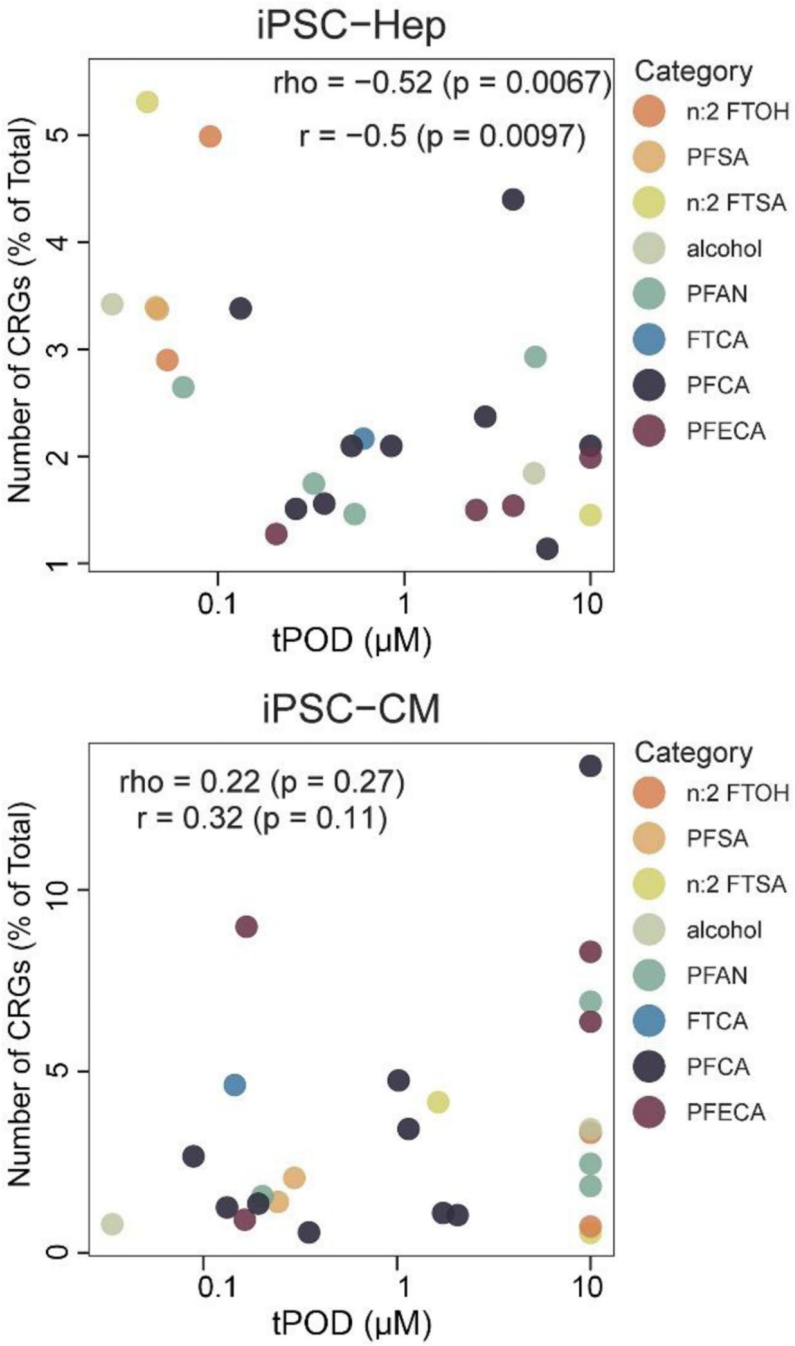

Fig. 7:

Correlations between transcriptomic Point of Departure (tPOD) and the number of concentration response genes (CRGs, expressed as a fraction of total genes retained after low count removal, as described in Methods) in iPSC-Hep (top) and iPSC-CM (bottom) treated with PFAS. Both Pearson (r) and Spearman (rho) correlations, and their corresponding p-values are displayed. Each data point represents a distinct PFAS, and the colors indicate different categories (as shown in the inset). See Tab. 1 for PFAS class abbreviations.

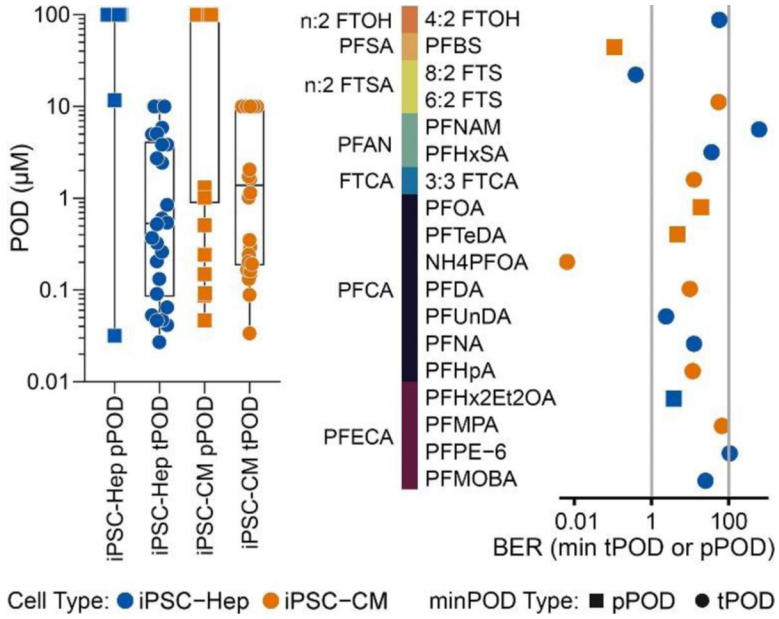

Fig. 8:

Comparisons of the points of departure (PODs) derived from phenotypic (pPOD) and transcriptomic (tPOD) data, and the calculated bioactivity-to-exposure ratios (BER) based on the lowest POD for each tested PFAS. **(A)** POD comparisons. Box-and-whisker plots illustrate the POD values derived from phenotypic data (indicated by solid squares) and transcriptomic data (indicated by solid circles) for iPSC-Hep (blue) and iPSC-CM (orange). The boxes represent the interquartile range, the horizontal line represents the median value, and the whiskers extend to encompass the maximum and minimum values. Values for each tested PFAS are shown as individual symbols. **(B)** A dot plot displaying the BERs calculated using the lowest (either pPOD or tPOD) values for each tested PFAS with available *in vitro*-to-*in vivo* extrapolation data. The solid dots and solid squares correspond to POD values from phenotypic and transcriptomic data, respectively. The blue and orange colors correspond to iPSC-Hep and iPSC-CM, respectively. The grey lines represent BER at 1 and 100. PFAS are grouped by their chemical structure-based class. See Tab. 1 for class and individual chemical abbreviations.

Table 1.

PFAS tested in this study.

CASRN	Chemical Name	Chemical Abbreviation	Category	Category Abbreviation
2043-47-2	4:2 Fluorotelomer alcohol	4:2 FTOH	n:2 Fluorotelomer alcohols	n:2 FTOH
678-39-7	8:2 Fluorotelomer alcohol	8:2 FTOH		
375-73-5	Perfluorobutanesulfonic acid	PFBS	Perfluoroalkane sulfonic acids/ perfluoroalkane sulfonates	PFSA
2806-15-7	Sodium perfluorodecanesulfonate	PFDS-Na		
39108-34-4	8:2 Fluorotelomer sulfonic acid	8:2 FTS	n:2 Fluorotelomer sulfonic acids	n:2 FTSA
27619-97-2	6:2 Fluorotelomer sulfonic acid	6:2 FTS		
355-80-6	1H,1H,5H-Perfluoropentanol	PFPOH	Alcohols	Alcohols
335-99-9	Dodecafluoroheptanol	DDFHp		
423-54-1	Perfluorooctanamide	PFOAM	Perfluoroalkane amide/amines	PFAN
13485-61-5	Nonafluoropentanamide	PFNAM		
41997-13-1	Perfluorohexanesulfonamide	PFHxSA		
307-31-3	Perfluorooctanamidine	PFOAMD		
356-02-5	3:3 Fluorotelomer carboxylic acid	3:3 FTCA	Fluorotelomer carboxylic acids	FTCA
335-67-1	Perfluorooctanoic acid	PFOA	Perfluoroalkyl carboxylic acids/ perfluoroalkyl carboxylates	PFCA
376-06-7	Perfluorotetradecanoic acid	PFTeDA		
72629-94-8	Perfluorotridecanoic acid	PFTiDA		
3825-26-1	Ammonium perfluorooctanoate	NH4PFOA		
335-76-2	Perfluorodecanoic acid	PFDA		
2058-94-8	Perfluoroundecanoic acid	PFUnDA		
375-95-1	Perfluorononanoic acid	PFNA		
1763-28-6	3,3-Bis(trifluoromethyl)-2-propenoic acid	TFPrOA		
375-85-9	Perfluoroheptanoic acid	PFHpA		
55621-21-1	Perfluoro-3,6-dioxaoctane-1,8-dioic acid	PFHx2Et2OA	Perfluoroalkyl ether carboxylic acids	PFECA
377-73-1	Perfluoro-3-methoxypropanoic acid	PFMPA		
330562-41-9	Perfluoro-3,6,9-trioxatridecanoic acid	PFPE-6		
863090-89-5	Perfluoro(4-methoxybutanoic) acid	PFMOBA		

Table 2.

Cell types used and *in vitro* readouts collected in this study.

Cell Type	Phenotype	Exposure Duration	Benchmark Response for POD Derivation
Human induced pluripotent stem cell-derived hepatocytes (iPSC-Hep)	Total Cell Number	48 hrs	1 SD
	Mitochondrial Integrity		
	Mitochondrial Intensity		
	Cytoplasmic Integrity		
	Cell Mean Area		
	Gene Expression		See Methods
Human induced pluripotent stem cell-derived cardiomyocytes (iPSC-CM)	Total Cell Number	90 mins	10% Change
	Positive Chronotropy		5% Change
	Negative Chronotropy		5% Change
	Asystole		95% Change
	QT Prolongation		5% Change
	Gene Expression	24 hrs	See Methods